iScience

CellPress
OPEN ACCESS

Article

SUFU suppresses ferroptosis sensitivity in breast cancer cells via Hippo/YAP pathway

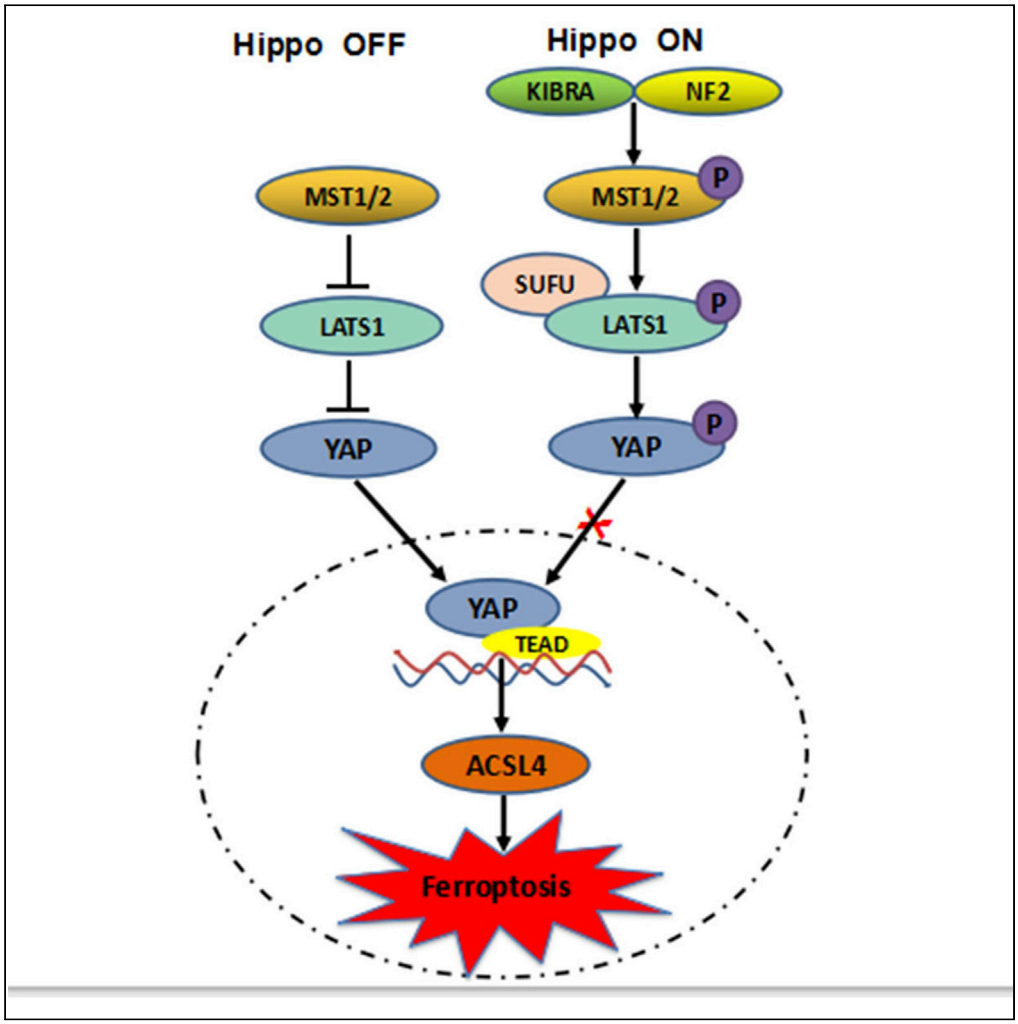

Kun Fang, Sha Du, Dachuan Shen, ..., Wei Cheng, Songshu Meng, Yifei Wang

jindi0801@126.com (D.J.)
wcheng@dmu.edu.cn (W.C.)
ssmeng@dmu.edu.cn (S.M.)
yly2000.312@163.com (Y.W.)

Highlights

SUFU regulates the sensitivity of breast cancer cells to ferroptosis

SUFU associates with LATS1 to downregulate the YAP-ACSL4 axis

Vincristine targets the SUFU-YAP-ACSL4 axis

Fang et al., iScience 25, 104618
July 15, 2022
https://doi.org/10.1016/j.isci.2022.104618

iScience

CellPress
OPEN ACCESS

Article

SUFU suppresses ferroptosis sensitivity in breast cancer cells via Hippo/YAP pathway

Kun Fang,[1,2,7] Sha Du,[2,7] Dachuan Shen,[3,7] Zhipeng Xiong,[2,7] Ke Jiang,[4,7] Dapeng Liang,[2] Jianxin Wang,[2] Huizhe Xu,[5] Lulu Hu,[6] Xingyue Zhai,[2] Yuting Jiang,[2] Zhiyu Xia,[2] Chunrui Xie,[2] Di Jin,[2,*] Wei Cheng,[2,*] Songshu Meng,[2,8,*] and Yifei Wang[1,*]

SUMMARY

Ferroptosis is a new kind of regulated cell death that is characterized by highly iron-dependent lipid peroxidation. Cancer cells differ in their sensitivity to ferroptosis. Here we showed that the Suppressor of fused homolog (SUFU), a critical component in Hedgehog signaling, regulates ferroptosis sensitivity of breast cancer cells. Ectopic SUFU expression suppressed, whereas depletion of SUFU enhanced the sensitivity of breast cancer cells to RSL3-triggered ferroptosis through deregulation of ACSL4. Moreover, SUFU depletion promoted the activation of Yes-associated protein (YAP), thereby increasing the expression of ACSL4. Mechanistically, SUFU is associated with LATS1. Deletion of a region comprising residues 174–385 in SUFU disrupted SUFU binding to LATS1, thus abrogating SUFU-mediated downregulation of the YAP-ACSL4 axis and sensitivity to ferroptosis. Noteworthy, we showed that vincristine downregulated SUFU, thus increasing breast cancer cell sensitivity to RSL3 *in vitro* and *in vivo*. Together, our findings uncover SUFU as a novel regulator in ferroptosis sensitivity.

INTRODUCTION

Ferroptosis is a non-apoptotic form of regulated cell death characterized by iron dependency and lipid peroxidation (Dixon et al., 2012). To date, only a few key molecular players which involved in ferroptosis such as the phospholipid hydroperoxide glutathione peroxidase (GPX4), cystine/glutamate transporter (SLC7A11), and the acyl-CoA synthetase long-chain family member 4 (ACSL4) have been identified (Dixon et al., 2012; Doll et al., 2017; Poursaitidis et al., 2017). Ferroptosis sensitivity varies markedly among cancer cells from distinct tissue lineages (Hangauer et al., 2017; Yang and Stockwell, 2008; Yi et al., 2020; Zhang et al., 2019). Hence, the understanding of the molecular mechanisms underlying ferroptosis sensitivity will be of significance. The transcriptional co-activators Yes-associated protein (YAP) and its paralog, transcriptional co-activator with the PDZ binding motif (TAZ; encoded by WWTR1), two effectors of the Hippo pathway, has been shown recently to be associated with sensitivity to ferroptosis (Gao et al., 2021; Lin et al., 2021; Wu et al., 2019; Yang and Chi, 2020; Yang et al., 2019, 2021; Zhang et al., 2021). For instance, YAP promotes ferroptosis by upregulating several ferroptosis modulators, including ACSL4 and transferrin receptor 1 (TFRC) in breast and colorectal cancer cells(Wu et al., 2019). In addition, the TAZ-EMP1-NOX4 axis upregulates ferroptosis sensitivity in renal cell carcinoma (Yang et al., 2019). In epithelial ovarian cancer cells, TAZ modulates ferroptotic cell death through the ANGPTL4–NOX2 axis (Yang et al., 2020). These studies highlight targeting the Hippo/YAP signaling might provide therapeutic potential for ferroptosis-inducing cancer therapy. However, the mechanisms underlying the regulation of YAP/TAZ signaling in ferroptosis remain unclear.

The Suppressor of fused homolog (SUFU) is known as a critical component in Hedgehog (Hh) signaling and has been implicated in cancer development (Alimirah et al., 2016; Kasai et al., 2008; Lee et al., 2007; Raducu et al., 2016). In the current study, we show that SUFU regulates ferroptosis sensitivity in breast cancer cells through the Hippo/YAP pathway.

RESULTS

SUFU suppresses the sensitivity of breast cancer cells to RSL3-induced ferroptosis

To date, whether Hh signaling or components regulate ferroptosis remains unknown. We systematically correlated sensitivity data (determined by the area under the curve (AUC)) of the ferroptosis inducers

[1]Department of Obstetrics and Gynecology, the Second Affiliated Hospital of Dalian Medical University, Dalian 116027, China

[2]Institute of Cancer Stem Cell, Dalian Medical University Cancer Center, No. 9 West Section, South Lvshun Road, Dalian 116044, China

[3]Department of Oncology, Affiliated Zhongshan Hospital of Dalian University, Dalian 116001, China

[4]Center for Single-Cell Omics, Shanghai Jiao Tong University School of Medicine, Shanghai 200025, China

[5]Central Laboratory, Cancer Hospital of China Medical University, Liaoning Cancer Hospital and Institute, Shenyang 110042, China

[6]Department of Clinical Laboratory, Qingdao Municipal Hospital, Qingdao University, Qingdao 266000, China

[7]These authors contributed equally

[8]Lead contact

*Correspondence: jindi0801@126.com (D.J.), wcheng@dmu.edu.cn (W.C.), ssmeng@dmu.edu.cn (S.M.), yly2000.312@163.com (Y.W.)

https://doi.org/10.1016/j.isci.2022.104618

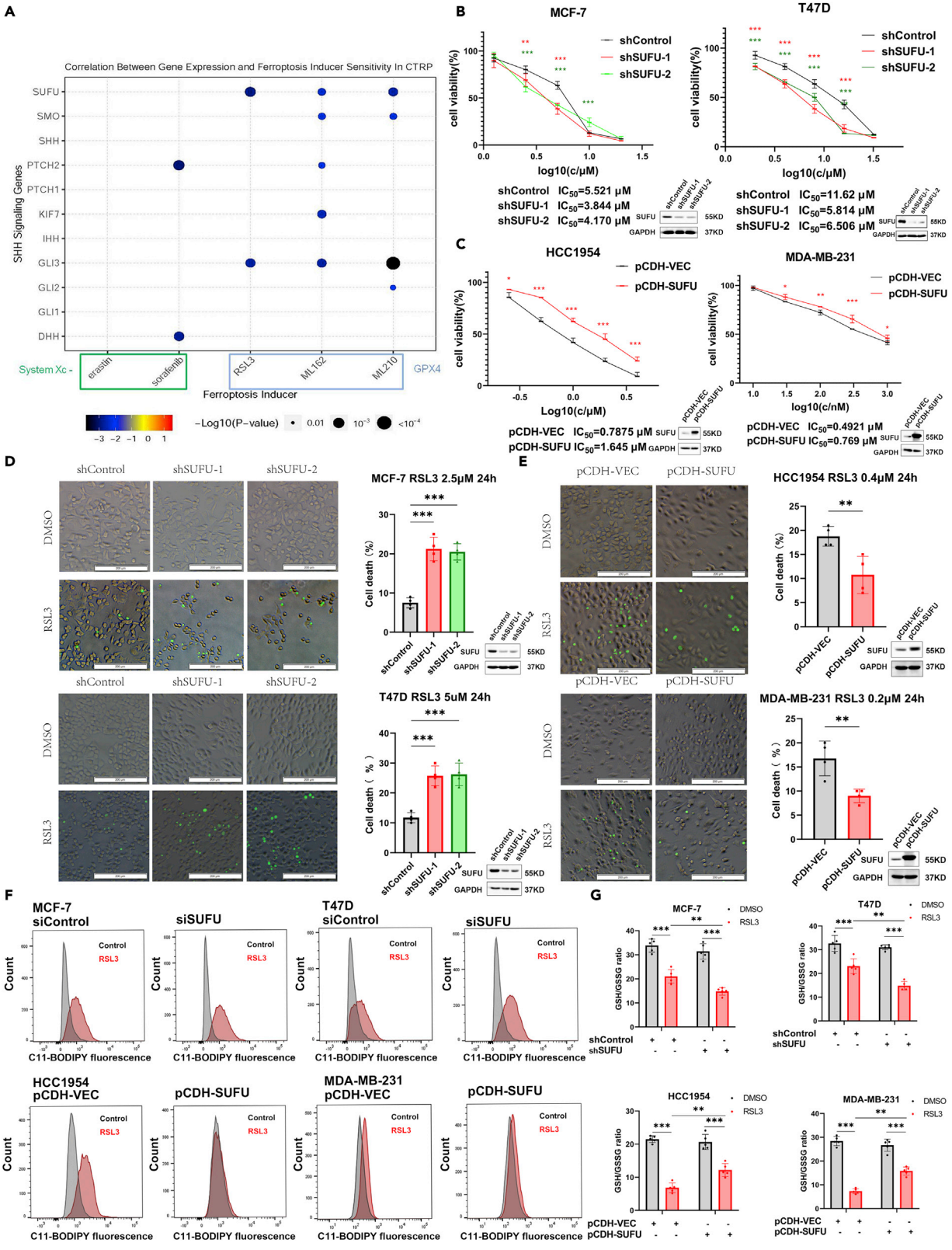
A
Correlation Between Gene Expression and Ferroptosis Inducer Sensitivity In CTRP
SHH Signaling Genes
SUFU
SMO
SHH
PTCH2
PTCH1
KIF7
IHH
GLI3
GLI2
GLI1
DHH
System Xc -
erastin
sorafenib
RSL3
ML162
ML210
GPX4
Ferroptosis Inducer
-Log10(P-value)
B
MCF-7
T47D
shControl
shSUFU-1
shSUFU-2
cell viability(%)
log10(c/μM)
shControl IC50=5.521 μM
shSUFU-1 IC50=3.844 μM
shSUFU-2 IC50=4.170 μM
shControl IC50=11.62 μM
shSUFU-1 IC50=5.814 μM
shSUFU-2 IC50=6.506 μM
SUFU
GAPDH
55KD
37KD
C
HCC1954
MDA-MB-231
pCDH-VEC
pCDH-SUFU
log10(c/nM)
pCDH-VEC IC50=0.7875 μM
pCDH-SUFU IC50=1.645 μM
pCDH-VEC IC50=0.4921 μM
pCDH-SUFU IC50=0.769 μM
D
shControl
shSUFU-1
shSUFU-2
DMSO
RSL3
MCF-7 RSL3 2.5μM 24h
T47D RSL3 5uM 24h
Cell death (%)
E
pCDH-VEC
pCDH-SUFU
HCC1954 RSL3 0.4μM 24h
MDA-MB-231 RSL3 0.2μM 24h
F
MCF-7
siControl
siSUFU
T47D
HCC1954
pCDH-VEC
pCDH-SUFU
MDA-MB-231
Control
RSL3
Count
C11-BODIPY fluorescence
G
GSH/GSSG ratio
shControl
shSUFU
pCDH-VEC
pCDH-SUFU
DMSO
RSL3

Figure 1. SUFU regulates the sensitivity of breast cancer cells to RSL3-triggered ferroptosis

(A) Pharmaco-transcriptomic correlation analysis identified key components of the SHH pathway associated with sensitivity to ferroptosis inducers across solid cancer cell lines (n = 658). Blue dots indicate the significantly negatively correlated genes while red dots indicate the positively correlated ones. Here, a negative correlation indicates the association of a larger AUC (area under the curve) with lower gene expression and vice versa.

(B and C) Viability (%) of breast cancer cells MCF-7 and T47D stably depleted of SUFU (B), or HCC1954 and MDA-MB-231 stably overexpressing SUFU (C), following RSL3 treatment at indicated concentrations for 24 h.

(D and E) Cell death determined by Sytox Green staining of cells in D and E, respectively, cells were treated with RSL3 at indicated concentrations for 24 h; scale bar, 200μm.

(F and G) RSL3-induced ROS levels (F) and GSH/GSSG ratios (G) were measured in MCF-7 and T47D cells in which SUFU was knocked down by siRNA (upper panels), or HCC1954 and MDA-MB-231 cells overexpressing SUFU (lower panels). ROS levels were assessed by flow cytometry with C11-BODIPY. GSH/GSSG ratios were measured by a GSH/GSSG-Glo assay. Data are presented as mean ± SD (*p < 0.05, **p < 0.01, ***p < 0.001, one-way ANOVA with Tukey's multiple comparisons test or Unpaired t test). Data are presented as mean ± SD (*p < 0.05, **p < 0.01, ***p < 0.001). (one-way ANOVA with Tukey's multiple comparisons test or Unpaired t test).

with key components of Hh signaling gene expression across the entire cancer cell line cohort. This analysis revealed that the mRNA expression level of SUFU most strongly correlated with the AUC of RSL3 (Figure 1A), a ferroptosis inducer that inhibits GPX4 (Yang et al., 2014). A significant correlation between SUFU expression and AUC of the other two covalent GPX4 inhibitors ML162 and ML210 was also detected. We thus hypothesized that SUFU expression would regulate cancer cell sensitivity to RSL3-induced ferroptosis. As documented in recent studies (Wu et al., 2019; Yi et al., 2020), MDA-MB-231 and HCC1954 breast cancer cell lines are sensitive (Doll et al., 2017; Hangauer et al., 2017; Hasegawa et al., 2016; Kraft et al., 2020), whereas MCF-7, SK-BR-3 and T47D cells are resistant (Hangauer et al., 2017; Kraft et al., 2020), to RSL3. Indeed, the half-maximal growth-inhibitory concentration (IC_{50}) analysis showed that HCC1954 and MDA-MB-231 cells were sensitive to RSL3 at concentrations less than 1μM, whereas MCF-7, SK-BR-3, and T47D cells were insensitive to RSL3 at concentrations around 5–11 μM (Figure S1A). Noteworthy, RSL3-induced cell death in the tested breast cancer cells was significantly suppressed by either ferrostatin-1 (Fer-1) or liproxstatin-1(Lipo-1), two ferroptosis inhibitors (Dixon et al., 2012; Friedmann Angeli et al., 2014), rather than by 3-Methyladenine (3-MA, an autophagy inhibitor), Z-VAD-FMK (an apoptosis inhibitor), or necrostatin-1 (a necrosis inhibitor) (Figure S1B), confirming the occurring of ferroptosis. We examined the expression of SUFU in a panel of breast cancer cell lines (Figure S1C) and stably knocked down SUFU with lentiviruses expressing shRNA or stably overexpressing a Flag-tagged SUFU cDNA construct in the tested cells (Figure S1D). Next, CCK-8 assay analysis showed that SUFU depletion in MCF-7 and T47D cells significantly increased (Figure 1B), whereas SUFU overexpression in HCC1954 and MDA-MB-231 cells significantly reduced the cell death induced by RSL3 (Figure 1C), compared with their corresponding controls. A similar effect was further validated by SYTOX Green cell death assay (Figures 1D and 1E) and crystal violet staining (Figures S1E and S1F) respectively. Noteworthy, the increased cell death upon RSL3 treatment by ablation of SUFU in MCF-7 and T47D cells was reversed by either Fer-1 or re-expression of a V5-tagged SUFU cDNA construct in these SUFU-depleted cells (Figures S1G and S1H).

The production of the lipid-based reactive oxygen species (lipid ROS), is a hallmark of ferroptosis. Lipid oxidation can be measured by staining with C11-BODIPY, a dye that detects lipid ROS in cell membranes. This experiment demonstrated that RSL3-induced accumulation of lipid ROS was elevated in both MCF-7 and T47D cells upon transient knockdown of SUFU with siRNA targeting SUFU, compared to non-targeting siRNA controls (Figure 1F, upper panels). On the contrary, ectopic expression of SUFU in HCC1954 and MDA-MB-231 cells led to a significant decrease in ROS levels induced by RSL3 (Figure 1F, lower panels). Oxidized form glutathione (GSSG) is one of the end products of lipid peroxidation during ferroptosis (Stockwell et al., 2020). GSH/GSSG-Glo assay revealed that SUFU overexpression significantly reversed the decreased GSH/GSSG ratio induced by RSL3 in HCC1954 and MDA-MB-231 cells (Figure 1G, lower panels), whereas depletion of SUFU in MCF-7 and T47D cells decreased further the GSH/GSSG ratio by RSL3 (Figure 1G, upper panels), comparing with their respective controls. Knockdown or overexpression of SUFU in these cells was confirmed by immunoblot assay (Figures S1I and S1J). Together, these data support that SUFU regulates the susceptibility of breast cancer cells to RSL3-triggered ferroptosis.

SUFU mediates resistance to RSL3-induced ferroptosis via downregulation of ACSL4

To explore the mechanistic connection between SUFU and ferroptosis, we performed RNA-seq analysis of control and SUFU-overexpressing SK-BR-3 cells (GEO accession number: GSE188806) and found 53 differentially expressed genes (oeSUFU-DE-Gs) (Table S1. Differentially expressed genes upon overexpression of SUFU compared to control in SK-BR-3 cells. Related to Figure 2). Among those oeSUFU-DE-Gs, three

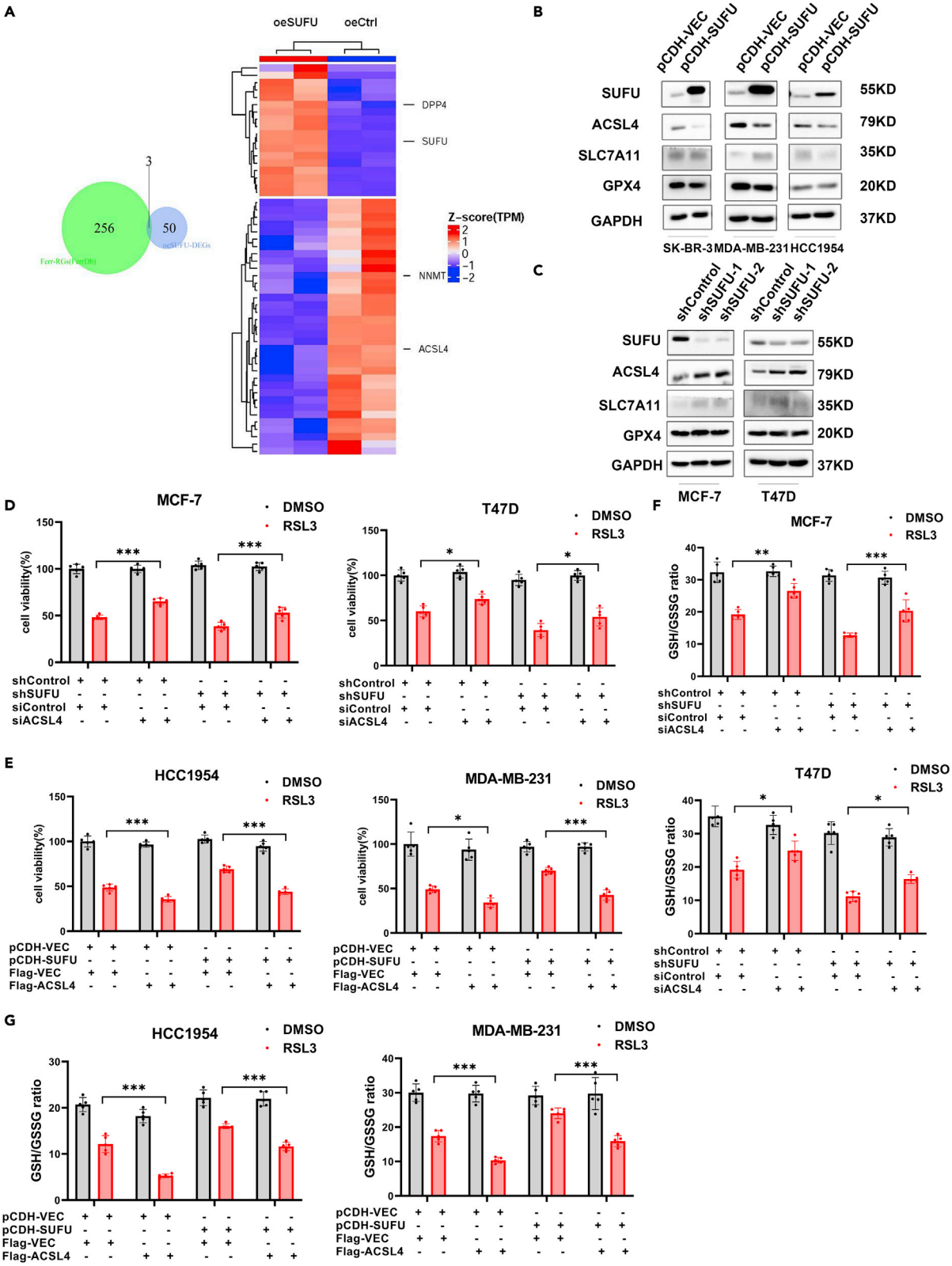
A
oeSUFU
oeCtrl
DPP4
SUFU
NNMT
ACSL4
Z-score(TPM)
2
1
0
−1
−2
3
256
50
oeSUFU-DEGs
B
pCDH-VEC
pCDH-SUFU
SUFU
ACSL4
SLC7A11
GPX4
GAPDH
55KD
79KD
35KD
20KD
37KD
SK-BR-3
MDA-MB-231
HCC1954
C
shControl
shSUFU-1
shSUFU-2
MCF-7
T47D
D
MCF-7
T47D
DMSO
RSL3
cell viability(%)
shControl
shSUFU
siControl
siACSL4
E
HCC1954
MDA-MB-231
T47D
pCDH-VEC
pCDH-SUFU
Flag-VEC
Flag-ACSL4
F
GSH/GSSG ratio
G

Figure 2. ACSL4 is critical for SUFU-mediated resistance to RSL3-induced ferroptosis

(A) Venn diagram of differentially expressed genes (oeSUFU-DE-Gs) between oeSUFU and oeControl SK-BR-3 cells as well as ferroptosis regulator genes (Ferr-RGs) recorded in the FerrDb database (Table S1). Overlapping genes (ACSL4, NNMT, DPP4) and SUFU were highlighted and labeled with gene symbols in the heatmap. The color bar denotes the *Z* score normalized TPM (Transcript Per Million) expression value.

(B and C) The levels of ferroptosis mediators including ACSL4, GPX4, and SLC7A11 in breast cancer cells upon SUFU overexpression (B) or SUFU depletion (C) were determined by immunoblot (IB) assay.

(D and F) Cell viability (D) and GSH/GSSG ratios (F) of SUFU-depleted MCF-7 and T47D cells in the absence or presence of RSL3 upon knockdown of ACSL4 using siRNA.

(E and G) Cell viability (E) and GSH/GSSG ratios (G) of SUFU-overexpressed HCC1954 and MDA-MB-231 cells in the absence or presence of RSL3 upon ectopic expression of ACSL4. Data are presented as mean ± SD (*$p < 0.05$, **$p < 0.01$, ***$p < 0.001$, Unpaired t test).

ferroptosis regulator genes (Ferr-RGs) recorded in the FerrDb database, including ACSL4, NNMT, and DPP4, were identified (Figure 2A). ACSL4, a ferroptosis mediator (Doll et al., 2017), was further investigated. We validated decreased ACSL4 protein abundance in SUFU-overexpressing SK-BR-3 cells. In addition, we observed decreased protein levels of ACSL4 in MDA-MB-231 and HCC1954 cells with SUFU overexpression (Figure 2B). By contrast, ACSL4 protein levels were substantially elevated in SUFU-depleted MCF-7 and T47D cells (Figure 2C). Of note, GPX4 or SLC7A11 protein levels were not substantially altered in these settings (Figures 2B and 2C). Moreover, ACSL4 abundance was markedly increased in tumor sections from mice bearing tumors derived from SUFU-depleted MDA-MB-231 cells (Figure S2A, lower panel). As expected, nude mice inoculated with SUFU-depleted MDA-MB-231 cells showed a significant increase in tumor growth compared to the control group (Figure S2A, upper panel), in line with that SUFU functions as a tumor suppressor.

ACSL4 predicts sensitivity to RSL3-triggered ferroptosis in a panel of basal-like breast cancer cell lines and sensitizes breast cancer cells to ferroptosis (Doll et al., 2017). The ACSL4 expression in a panel of breast cancer cell lines was examined by IB (Figure S2B). We stably ablated ACSL4 expression in MDA-MB-231 and HCC1954 cells using lentiviruses expressing shRNA targeting ACSL4 (Figure S2C) and treated these cells with RSL3 for 24h. As expected, ACSL4 depletion markedly mitigated RSL3-induced cell death in MDA-MB-231 and HCC1954 cells (Figure S2D), confirming an essential role of ACSL4 in RSL3-induced ferroptosis. Moreover, upon RSL3 exposure, the increase in ferroptosis caused by SUFU ablation in MCF-7 and T47D cells were significantly mitigated by siRNA-mediated knockdown of ACSL4 (Figure 2D), whereas the decrease in ferroptosis caused by SUFU overexpression in HCC1954 and MDA-MB-231 cells was rescued by ectopic ACSL4 expression (Figure 2E). Consistently, ACSL4 knockdown significantly abrogated SUFU depletion-induced decrease in the GSH/GSSG ratio upon RSL3 treatment (Figure 2F), whereas forced expression of a Flag-tagged ACSL4 construct significantly mitigated SUFU overexpression-induced increase in the GSH/GSSG ratio in the presence of RSL3 (Figure 2G). Ectopic expression or siRNA-mediated knockdown of ACSL4 in these breast cancer cells were examined by IB respectively (Figure S2E).

SUFU depletion upregulates YAP activity and target gene expression

To gain insights into how SUFU regulates ACSL4 expression in breast cancer cells, we analyzed differential gene expression between SUFU-depleted and shControl HCC1954 cells (GEO accession number: GSE188806). Gene set enrichment analysis (GSEA) using a curated set of YAP-dependent signatures showed that depletion of SUFU in HCC1954 cells results in a highly significant enrichment of active YAP gene expression signatures (Figure 3A and Table S2. Differentially expressed genes upon knockdown of SUFU compared to control in HCC1954 cells. And Table S3. Gene set enrichment analysis (GSEA) of YAP gene set upon knockdown of SUFU in HCC1954 cells. Related to Figure 3, $p < 0.05$, $q < 0.25$). AXL as a YAP-dependent target gene, was highlighted in the display (Figure 3A). IB analysis showed a robust upregulation of AXL and ACSL4, two YAP-regulated genes (Wu et al., 2019), in SUFU-depleted HCC1954, MCF-7, and MDA-MB-231 cells (Figure 3B). Importantly, re-expression of V5-tagged SUFU in these SUFU-depleted cells robustly restored the levels of AXL and ACSL4 to the control level (Figure 3C), indicating that the increase in the levels of AXL and ACSL4 upon SUFU knockdown is a consequence of SUFU deficiency. Consistently, overexpression of SUFU in HCC1954, MDA-MB-231, and SK-BR-3 cells led to a marked decrease in the protein levels of AXL and ACSL4 (Figure S3A), suggesting that SUFU elevation is sufficient to downregulate YAP activity in breast cancer cells. To further confirm this notion, breast cancer cells with SUFU manipulation were transfected with a reporter encoding a YAP/TAZ-responsive luciferase gene (8xGTIIC-luciferase reporter), in which eight TEAD-YAP-binding sites were cloned into a promoter which drives the expression of firefly luciferase (Dupont et al., 2011). We found that SUFU depletion in HCC1954 and MCF-7 cells exhibited a significantly increased expression from the luciferase reporter

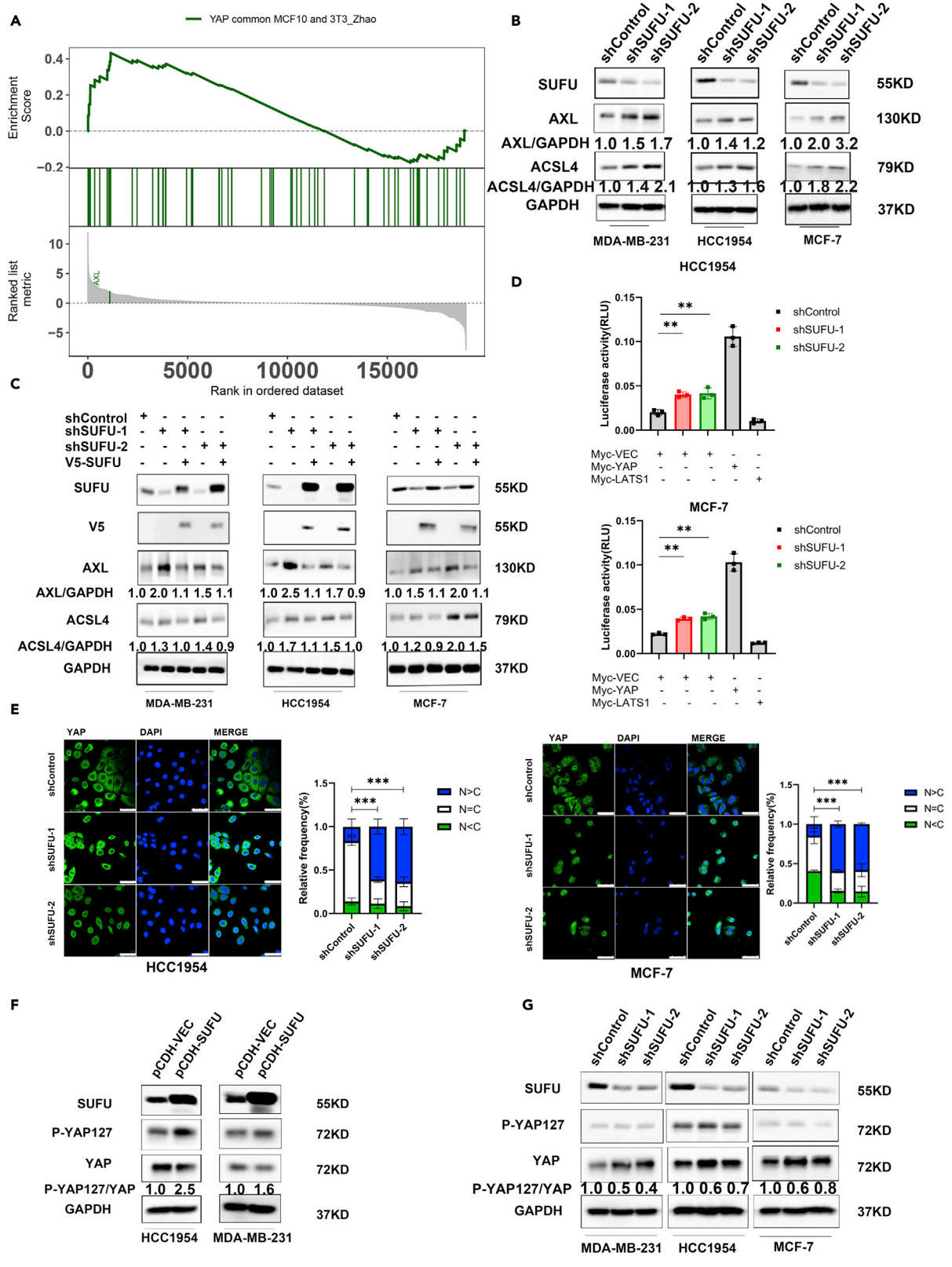
A
YAP common MCF10 and 3T3_Zhao
Enrichment Score
Ranked list metric
AXL
Rank in ordered dataset
B
shControl
shSUFU-1
shSUFU-2
SUFU
AXL
AXL/GAPDH 1.0 1.5 1.7 1.0 1.4 1.2 1.0 2.0 3.2
ACSL4
ACSL4/GAPDH 1.0 1.4 2.1 1.0 1.3 1.6 1.0 1.8 2.2
GAPDH
55KD
130KD
79KD
37KD
MDA-MB-231
HCC1954
MCF-7
C
shControl
shSUFU-1
shSUFU-2
V5-SUFU
SUFU
V5
AXL
AXL/GAPDH 1.0 2.0 1.1 1.5 1.1 1.0 2.5 1.1 1.7 0.9 1.0 1.5 1.1 2.0 1.1
ACSL4
ACSL4/GAPDH 1.0 1.3 1.0 1.4 0.9 1.0 1.7 1.1 1.5 1.0 1.0 1.2 0.9 2.0 1.5
GAPDH
55KD
55KD
130KD
79KD
37KD
MDA-MB-231
HCC1954
MCF-7
D
Luciferase activity(RLU)
shControl
shSUFU-1
shSUFU-2
Myc-VEC
Myc-YAP
Myc-LATS1
MCF-7
Luciferase activity(RLU)
shControl
shSUFU-1
shSUFU-2
Myc-VEC
Myc-YAP
Myc-LATS1
E
YAP
DAPI
MERGE
shControl
shSUFU-1
shSUFU-2
HCC1954
Relative frequency(%)
N>C
N=C
N<C
YAP
DAPI
MERGE
shControl
shSUFU-1
shSUFU-2
MCF-7
Relative frequency(%)
N>C
N=C
N<C
F
pCDH-VEC
pCDH-SUFU
SUFU
P-YAP127
YAP
P-YAP127/YAP 1.0 2.5 1.0 1.6
GAPDH
55KD
72KD
72KD
37KD
HCC1954
MDA-MB-231
G
shControl
shSUFU-1
shSUFU-2
SUFU
P-YAP127
YAP
P-YAP127/YAP 1.0 0.5 0.4 1.0 0.6 0.7 1.0 0.6 0.8
GAPDH
55KD
72KD
72KD
37KD
MDA-MB-231
HCC1954
MCF-7

Figure 3. SUFU downregulates YAP activity

(A) Gene set enrichment analysis (GSEA) of YAP target gene set upon knockdown of SUFU in HCC1954 cells. Gene symbols of the YAP common MCF10 and 3T3_Zhao gene set and detailed information on GSEA results were provided in Table S2. AXL, as a YAP-dependent target gene, was highlighted in the display.

(B and C) Immunoblot (IB) analysis of AXL and ACSL4 abundance upon SUFU depletion in HCC1954, MCF-7, and MDA-MB-231 cells (B). A rescue experiment was performed by ectopic expression of a V5-tagged SUFU construct in SUFU-depleted cells (C). GAPDH as a loading control. Numbers indicate the normalized ratio of ACSL4 or AXL over GAPDH signals obtained by densitometric analysis.

(D) Expression of TEAD luciferase reporter in SUFU-depleted MCF-7 and HCC1954 cells and their respective control cells. Cells were transfected with the 8xGTIIC-luciferase reporter and pRL-TK Renilla luciferase. Renilla luciferase was used as an internal control. Data were normalized to vector control.

(E) Confocal analysis of YAP nuclear localization in SUFU-depleted HCC1954 (left panels) and SUFU-depleted MCF-7 (right panels) cells; scale bar, 50μm.

(F and G) IB analysis of P-YAP127 and total YAP levels in SUFU-overexpressed HCC1954 and MDA-MB-231 cells (F), in SUFU-depleted HCC1954, MCF-7, and MDA-MB-231 cells (G). Densitometric analysis of the normalized ratio of P-YAP127 over total YAP signals was shown. Data are presented as mean ± SD (*$p < 0.05$, **$p < 0.01$, ***$p < 0.001$, one-way ANOVA with Tukey's multiple comparisons test).

(Figure 3D), whereas overexpression of SUFU in HCC1954, MDA-MB-231, and SK-BR-3 cells led to an opposite effect (Figure S3B), suggesting that SUFU indeed regulates YAP activity.

The increase in YAP activity upon SUFU depletion in breast cancer cells indicates YAP activation. To confirm this, we examined the nuclear localization of active YAP. Confocal analysis showed that depletion of SUFU led to significant increases in nuclear YAP in HCC1954 and MCF-7 cells (Figure 3E), whereas overexpression of SUFU resulted in significant decreases in nuclear YAP in these cells (Figure S3C), compared with their respective controls. Consistently, subcellular fractionation analysis revealed a remarkable decrease in nuclear YAP in SUFU-overexpressing HCC1954 and MCF-7 cells (Figure S3D). The phosphorylation status of YAP at Ser127, which is the LATS target site that mediates YAP cytoplasmic sequestration, is an indicator of YAP activation (Zhao et al., 2010). We observed an increase in P-YAP/YAP ratio in SUFU-expressing HCC1954 and MDA-MB-231 cells (Figure 3F). On the contrary, SUFU depletion led to a decrease in P-YAP/YAP ratio in HCC1954, MCF-7, and MDA-MB-231 cells (Figure 3G). Overall, these data reveal that SUFU plays a role in regulating YAP activation in at least breast cancer cells.

SUFU interacts with LATS1 to regulate YAP activity

We next dissect how SUFU regulates YAP activity in breast cancer cells. In the canonical Hippo pathway, YAP S127 phosphorylation is regulated by the MST/LATS kinase cascade. We found that SUFU overexpression led to an increase in P-LATS1/LATS1 ratio in HCC1954 and MDA-MB-231 cells (Figure 4A), whereas depletion of SUFU resulted in a decrease in P-LATS1/LATS1 ratio (Figure 4B). Surprisingly, SUFU overexpression induced a strong decrease in LATS1 abundance in HCC1954 and MDA-MB-231 cells, whereas SUFU ablation increased LAST1 abundance in these cells (Figures 4A and 4B). In addition, phosphorylation of MST1/2 remained unchanged upon SUFU overexpression or depletion in these cells (data not shown). Therefore, these data suggest that SUFU regulates LAST1 activity and/or abundance. To examine whether SUFU regulates YAP signaling via LATS1, we ectopically expressed SUFU in MDA-MB-231 and T47D cells with stable knockdown of LATS1. As expected, LATS1 knockdown led to the upregulation of YAP target genes AXL and ACSL4 (Figure 4C, comparing lane 1 with 2, three in left and right panels, respectively), whereas ectopic SUFU expression downregulated the levels of AXL and ACSL4 in control cells (Figure 4C, comparing lane 1 with 4 in left and right panels respectively). Notably, ectopic SUFU expression failed to impair the upregulation of AXL and ACSL4 in LATS1 knockdown cells (Figure 4C, comparing lane 4 with 5, six in left and right panels respectively), indicating that SUFU regulates YAP activity in a LATS1-dependent fashion.

We next examined how SUFU regulates the Hippo/YAP signaling by first testing for physical interaction between SUFU and key components of Hippo signaling including Merlin, Kibra, MST1/2, SAV1, LATS1/2, MOB1 as well as the Hippo effector YAP. Immunoprecipitation of V5-tagged-SUFU revealed that Myc-tagged LATS1, but not other tested Hippo components, robustly interacted with SUFU at the exogenous level in transfected HEK293T cells (Figures 4D and S4A). A faint interaction between merlin and SUFU at the exogenous level was also observed. In addition, we observed cytoplasmic co-localization between Flag-tagged SUFU and Myc-tagged LATS1 in MDA-MB-231 (Figure 4E) and MCF-7 cells (Figure S4B). Moreover, the physiologic association between endogenous SUFU and endogenous LATS1 was detected in HCC1806 cells (Figure 4F). To map the determinants of the interactions between SUFU and LATS1, we constructed a series of SUFU deletion mutants and assessed the interaction by immunoprecipitation and IB. A schematic depicting the regions in SUFU is shown in Figure 4G. As shown in Figure 4H, deletion of a region comprising residues 174–385 (hereafter as d174-385), but not other regions in SUFU, dramatically diminished its

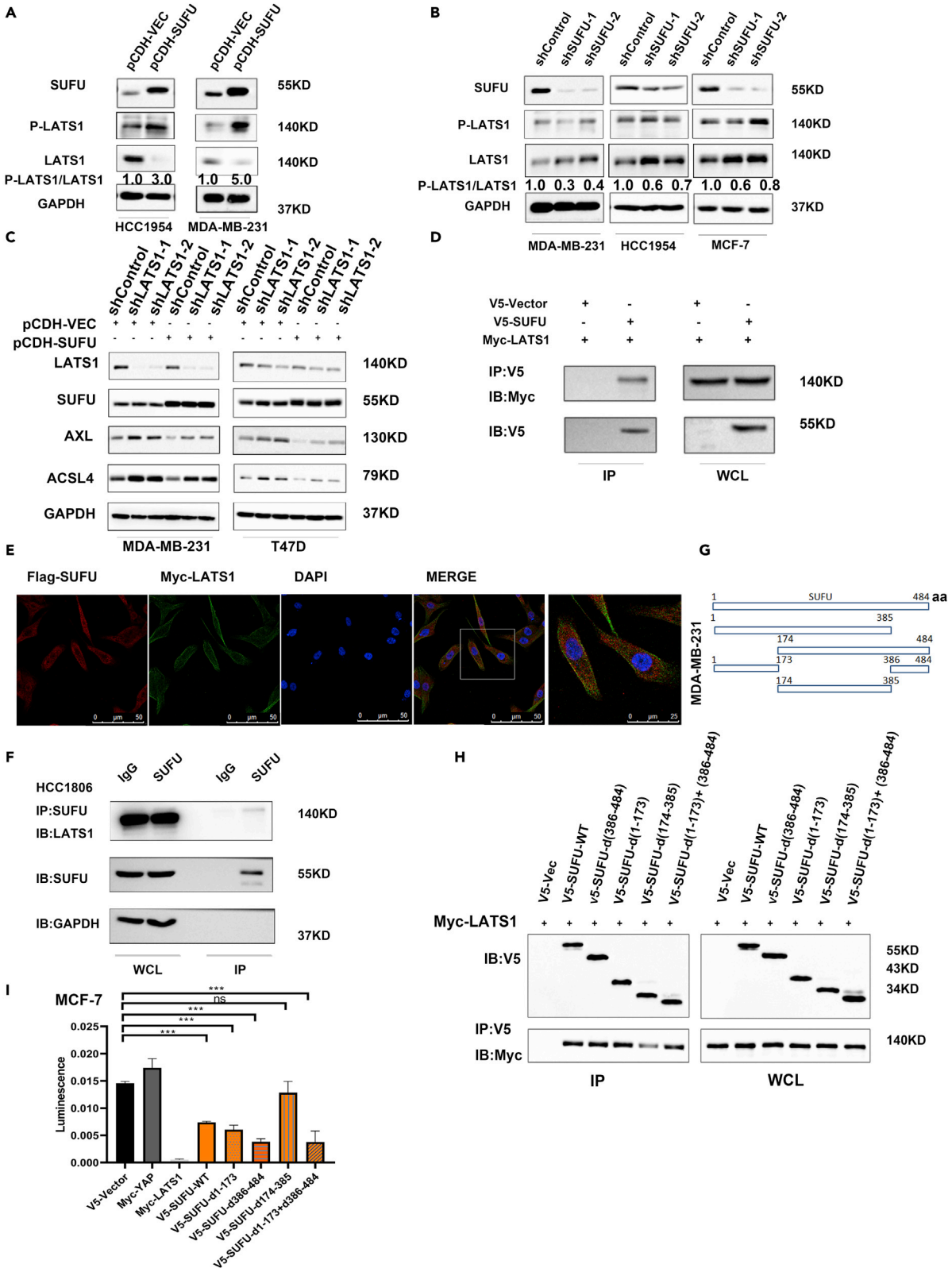
A
pCDH-VEC
pCDH-SUFU
SUFU
P-LATS1
LATS1
P-LATS1/LATS1
GAPDH
55KD
140KD
140KD
37KD
1.0 3.0
1.0 5.0
HCC1954
MDA-MB-231
B
shControl
shSUFU-1
shSUFU-2
SUFU
P-LATS1
LATS1
P-LATS1/LATS1
GAPDH
55KD
140KD
140KD
37KD
1.0 0.3 0.4
1.0 0.6 0.7
1.0 0.6 0.8
MDA-MB-231
HCC1954
MCF-7
C
shControl
shLATS1-1
shLATS1-2
pCDH-VEC
pCDH-SUFU
LATS1
SUFU
AXL
ACSL4
GAPDH
140KD
55KD
130KD
79KD
37KD
MDA-MB-231
T47D
D
V5-Vector
V5-SUFU
Myc-LATS1
IP:V5
IB:Myc
IB:V5
140KD
55KD
IP
WCL
E
Flag-SUFU
Myc-LATS1
DAPI
MERGE
G
MDA-MB-231
SUFU
484 aa
385
174
484
173
386
484
174
385
F
HCC1806
IgG
SUFU
IP:SUFU
IB:LATS1
IB:SUFU
IB:GAPDH
140KD
55KD
37KD
WCL
IP
H
V5-Vec
V5-SUFU-WT
V5-SUFU-d(386-484)
V5-SUFU-d(1-173)
V5-SUFU-d(174-385)
V5-SUFU-d(1-173)+ (386-484)
Myc-LATS1
IB:V5
IP:V5
IB:Myc
55KD
43KD
34KD
140KD
IP
WCL
I
MCF-7
***
ns
Luminescence
0.025
0.020
0.015
0.010
0.005
0.000
V5-Vector
Myc-YAP
Myc-LATS1
V5-SUFU-WT
V5-SUFU-d1-173
V5-SUFU-d386-484
V5-SUFU-d174-385
V5-SUFU-d1-173+d386-484

Figure 4. SUFU is associated with LATS1

(A and B) Immunoblot (IB) analysis of the levels of P-LATS1 and total LATS1 following SUFU overexpression (A) in HCC1954 and MDA-MB-231 cells or SUFU depletion (B) in HCC1954 MCF-7, and MDA-MB-231 cells. GAPDH as a loading control. Numbers indicate the normalized ratio of P-LATS1 over total LATS1 signals obtained by densitometric analysis.

(C) IB analysis of ACSL4 and AXL levels in LATS1-depleted MDA-MB-231 and T47D cells upon overexpressing SUFU. GAPDH as a loading control.

(D) HEK293T cells were transfected with indicated plasmids, cell lysates were subjected to immunoprecipitation (IP) with anti-V5 and IB with the antibodies against V5 and Myc, respectively.

(E) Confocal analysis of the co-localization of ectopic Flag-tagged SUFU and Myc-tagged LATS1 in MDA-MB-231 cells; scale bar, 50μm.

(F) HCC1806 whole-cell lysates (WCL) collected from 10cm^2 dishes were subjected to IP with an anti-SUFU antibody or IgG control. IB analysis for SUFU and LATS1. GAPDH as a loading control.

(G) A schematic depicting the regions in SUFU for mapping.

(H) IB analysis of V5-SUFU and its deletion mutants immunoprecipitated complexes using the indicated antibodies.

(I) Luciferase reporter assay analysis of the effects of SUFU wild type and its deletion mutants on YAP activity. MCF-7 cells were transfected with the 8xGTIIC-luciferase reporter together with SUFU wild type and its deletion mutants. Myc-tagged YAP and Myc-tagged LATS1 were used as the positive or negative control respectively. Data are presented as mean ± SD (*p < 0.05, **p < 0.01, ***p < 0.001, one-way ANOVA with Tukey's multiple comparisons test).

interaction with LATS1. We next examined the ability of SUFU deletion mutants in regulating YAP activity. The SUFU d174-385 deletion mutant which disrupts SUFU binding to LATS1 failed to inhibit the TEAD luciferase reporter activity as wild-type SUFU and other deletion mutants did in MCF-7 (Figure 4I), and HCC1954 (Figure S4C) cells. In addition, SUFU depletion-mediated increases in YAP nuclear localization as well as in the levels of AXL and ACSL4 in HCC1954 cells could not be rescued by the SUFU d174-385 deletion mutant (Figures S4D and S4E), while wild SUFU and other deletion mutants could do so.

SUFU modulates susceptibility of breast cancer cells to ferroptosis through YAP signaling

We next investigate whether SUFU regulates breast cancer cell growth and susceptibility to RSL3 through YAP signaling. To test this, we knocked down YAP with short interfering RNA (siRNA) in SUFU-depleted cells or treated the cells with verteporfin, which inhibits TEAD-YAP association thus disrupting YAP/TEAD-mediated transcription (Liu-Chittenden et al., 2012). As shown in Figure 5A, knockdown of YAP with siRNA markedly attenuated the increase in the levels of AXL and ACSL4 triggered by SUFU depletion in MDA-MB-231 and T47D cells. Similar effects were detected in SUFU-depleted HCC1954 and MDA-MB-231 cells treated with verteporfin (Figure 5B). Surprisingly, verteporfin robustly decreased SUFU abundance in control cells. YAP is phosphorylated on multiple serine residues by LATS1/2, and the conversion of all these serine residues into alanine creates constitutively active YAP (YAP5SA) mutant that are no longer inhibited by LATS1/2 (Zhao et al., 2007). The YAP S94A mutant without the TEAD binding site, selectively abolishes YAP's ability to activate TEADs (Zhao et al., 2008). We also employed another complementary method, i.e. ectopic expression of YAP-5SA or YAP-S94A in SUFU-overexpressing HCC1954 and MDA-MB-231 cells. Ectopic expression of YAP-5SA, but not YAP-S94A, substantially impaired the decrease in the levels of AXL and ACSL4 by SUFU overexpression (Figure 5C). Noteworthy, the increase in the sensitivity to RSL3 (i.e. more cell death) and the decrease in GSH/GSSG ratios caused by SUFU depletion in MCF-7 and T47D cells were reversed by YAP knockdown (Figures 5D and 5E), while the decreased sensitivity to RSL3 (i.e. less cell death) and the increased GSH/GSSG ratios by SUFU overexpression in HCC1954 and MDA-MB-231 cells were reverted by ectopic expression of YAP (Figures 5F and 5G). Knockdown or overexpression of YAP in the tested cell lines was examined by immunoblot assay (Figure 5H). Together, these data highlight that YAP abundance and activity are essential for SUFU-mediated effects on breast cancer cell growth and sensitivity to RSL3.

Vincristine downregulates SUFU and increases breast cancer cell sensitivity to RSL3

Our above findings suggest that targeting SUFU might enhance breast cancer cell sensitivity to RSL3. To obtain a pharmacologic modulation of SUFU expression, we tested several clinically relevant drugs including 5-fluorouracil, cisplatin, doxorubicin hydrochloride, metformin, paclitaxel, and vincristine. HCC1954, MCF-7, and MDA-MB-231 cells were treated with these compounds at different doses for 24h. Treatment with these compounds alone did not induce substantial cell death (data not shown). We found that among these tested drugs, vincristine (VCR) robustly decreased SUFU levels in all three cell lines (Figure 6A). Furthermore, VCR treatment led to a dose-dependent decrease in SUFU levels in HCC1954, MCF-7, and MDA-MB-231 cells with a concomitant decrease in P-YAP127 levels and an increase in AXL and ACSL4 levels (Figure 6B). In addition, VCR treatment also decreased the level of ectopic expressed SUFU in HCC1954 and MCF-7 cells with a concomitant increase in the levels of AXL and ACSL4 (Figure S5A). Moreover, we observed an increase in YAP nuclear localization upon VCR treatment in HCC1954 and MDA-MB-231 cells (Figure 6C). Noteworthy, siRNA-mediated knockdown of YAP abrogated VCR-induced

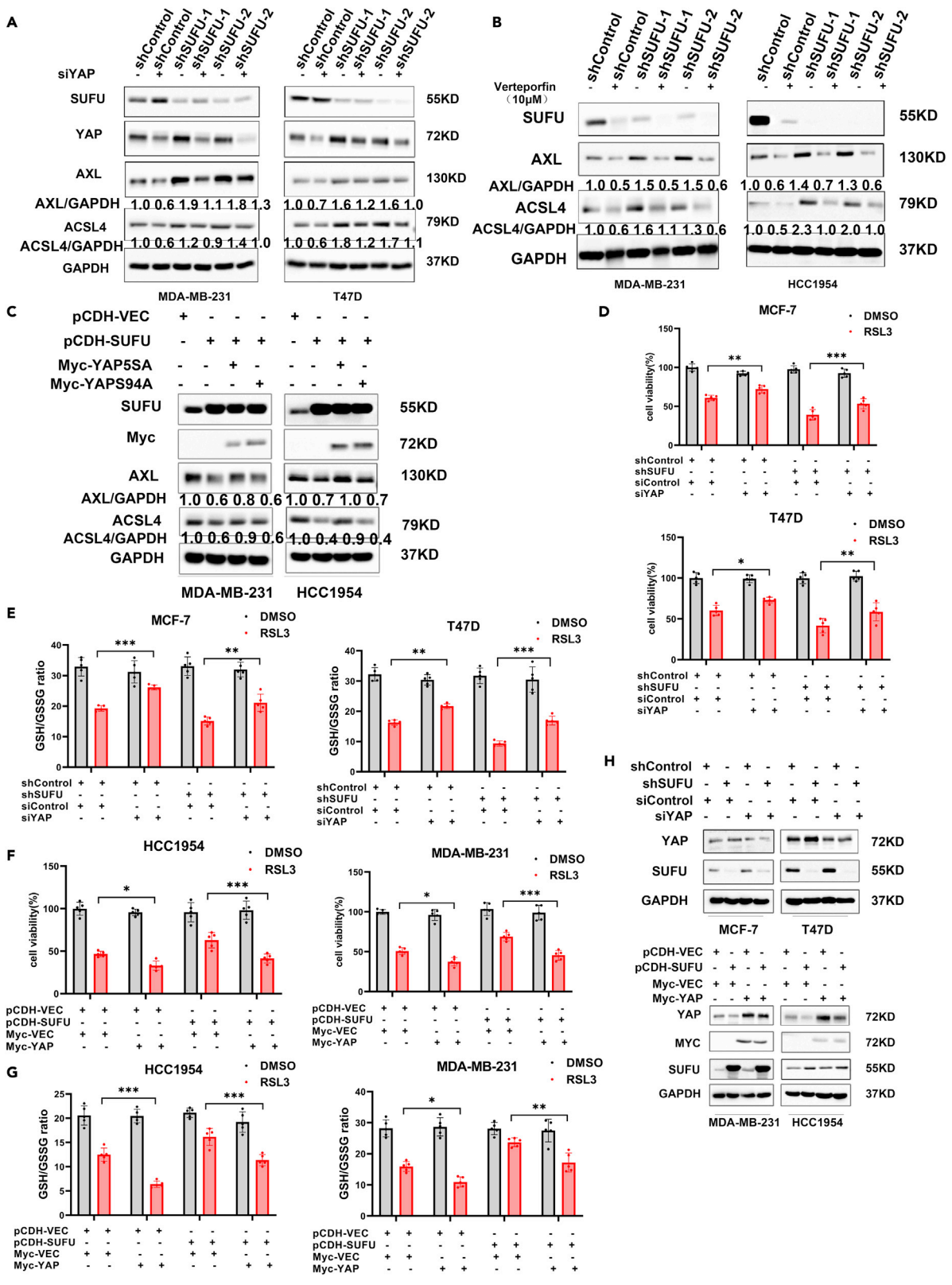
A
shControl
shSUFU-1
shSUFU-2
siYAP
SUFU
YAP
AXL
AXL/GAPDH
ACSL4
ACSL4/GAPDH
GAPDH
55KD
72KD
130KD
79KD
37KD
MDA-MB-231
T47D
B
Verteporfin (10μM)
HCC1954
C
pCDH-VEC
pCDH-SUFU
Myc-YAP5SA
Myc-YAPS94A
Myc
D
MCF-7
DMSO
RSL3
cell viability(%)
shControl
shSUFU
siControl
siYAP
E
GSH/GSSG ratio
F
pCDH-VEC
pCDH-SUFU
Myc-VEC
Myc-YAP
G
H
MYC

Figure 5. YAP is essential for SUFU-mediated insensitivity to RSL3

(A and B) Immunoblot (IB) analysis of AXL and ACSL4 levels in SUFU-depleted MDA-MB-231 and T47D cells upon YAP knockdown (A), and in SUFU-depleted HCC1954 and MDA-MB-231 cells treated with verteporfin (B), a YAP-TEAD inhibitor. Numbers indicate the normalized ratio of AXL or ACSL4 over GAPDH signals obtained by densitometric analysis.

(C) IB analysis of AXL and ACSL4 levels in SUFU-overexpressed HCC1954 and MDA-MB-231 cells upon ectopic expression of Myc-tagged YAP5SA (constitutively active YAP) or Myc-tagged YAPS94A (inability to bind TEAD). Numbers indicate densitometric analysis.

(D and E) Sensitivity to RSL3 (D), and GSH/GSSG ratios (E) of SUFU-depleted MCF-7 and T47D cells upon siRNA-mediated knockdown of YAP.

(F and G) Sensitivity to RSL3 (F), and GSH/GSSG ratios (G) of SUFU-overexpressed HCC1954 and MDA-MB-231 cells upon ectopic expression of Myc-tagged YAP.

(H) IB analysis of YAP expression in the indicated cells upon YAP knockdown or overexpression. GAPDH as a loading control. Data are presented as mean ± SD (*$p < 0.05$, **$p < 0.01$, ***$p < 0.001$, Unpaired t test).

increases in the levels of AXL and ACSL4 in HCC1954 and MDA-MB-231 cells (Figure 6D), while VCR-triggered downregulation of SUFU was not affected by YAP knockdown. Altogether, these data suggest that VCR might upregulate the YAP-ACSL4 axis at least partly via targeting SUFU.

Next, we asked whether VCR would increase breast cancer cell sensitivity to RSL3. We observed that combined treatment with VCR and RSL3 resulted in synergistic response in MCF-7 and T47D cells which are insensitive to RSL3 (Figure 6E), while no significant cell death was observed when treated with VCR or RSL3 alone. Notably, the combination of VCR and RSL3 significantly enhanced YAP nuclear localization in MCF-7 cells compared with RSL3 alone treatment (Figure S5B). Finally, mice bearing MCF-7-derived tumors were used to evaluate the *in vivo* response to RSL3 and VCR. RSL3 at high concentrations significantly suppressed tumor growth compared to either vehicle or RSL3 at low concentrations. However, the combination of VCR and RSL3 resulted in significant tumor regression compared with any single modality (RSL3 at low concentrations) (Figures 6F and S6A). IHC analysis revealed a decrease in both Ki67 and SUFU staining and an increase in ACSL4 staining in tumor sections from mice treated with the combination of VCR and RSL3, compared with the drug alone group (Figure 6G).

DISCUSSION

Here, we show that SUFU, a key component of Hh signaling, suppresses the sensitivity of breast cancer cells to RSL3-induced ferroptosis. Mechanistically, SUFU interacts with LATS1 thus downregulating the YAP-ACSL4 axis. We further demonstrate that targeting SUFU may represent a strategy to sensitize breast cancer cells to ferroptosis induction.

Ferroptosis is increasingly recognized as a promising avenue to kill cancers resistant to standard treatments. However, regulators that predict the sensitivity and/or resistance of ferroptosis and the underlying mechanisms are not yet completely investigated. Recent studies reported that the Hippo/YAP pathway regulates ferroptosis sensitivity in several types of cancer such as mesothelioma (Wu et al., 2019), ovarian cancer (Yang et al., 2020), and renal cell carcinoma (Yang et al., 2019). Thus, modulators of the Hippo/YAP pathway might be related to ferroptosis sensitivity. Supporting this notion, we revealed that SUFU regulates breast cancer cell sensitivity to RSL3-triggered ferroptosis via perturbing the Hippo/YAP signaling, as demonstrated by our gain- and loss-of-function analyses. Given that SUFU acts primarily as a negative regulator of the Hh signaling pathway via interacting with Gli proteins (Kim et al., 2019), our findings uncover a new mechanism of action for SUFU in cancer.

Our findings suggest that elevated SUFU in breast cancer might serve as a predictor for responsiveness to ferroptosis induction for at least RSL3. We recently reported that SASH1 suppressed breast cancer cell invasiveness by targeting the Hippo/YAP pathway (Jiang et al., 2020). It will be interesting to investigate whether SASH1 and other reported modulators of the Hippo/YAP signaling would contribute to the ferroptosis sensitivity in cancer. In search of potential avenues to overcome SUFU-mediated resistance to RSL3, we screened out vincristine, which could target SUFU and its regulated YAP-ACSL4 axis among several clinically relevant chemotherapeutic agents. Currently, vincristine is mostly used in combination with other anti-cancer drugs in active clinical trials (Skubnik et al., 2021), therefore our finding may have potential implications for ferroptosis-inducing cancer therapies.

To be taken together, our study demonstrates for the first time a crucial role for SUFU in regulating ferroptosis sensitivity in breast cancer cells. We suggest that vincristine warrants further clinical development in combination with RSL3 for the treatment of breast cancer that is insensitive to RSL3-triggered ferroptosis.

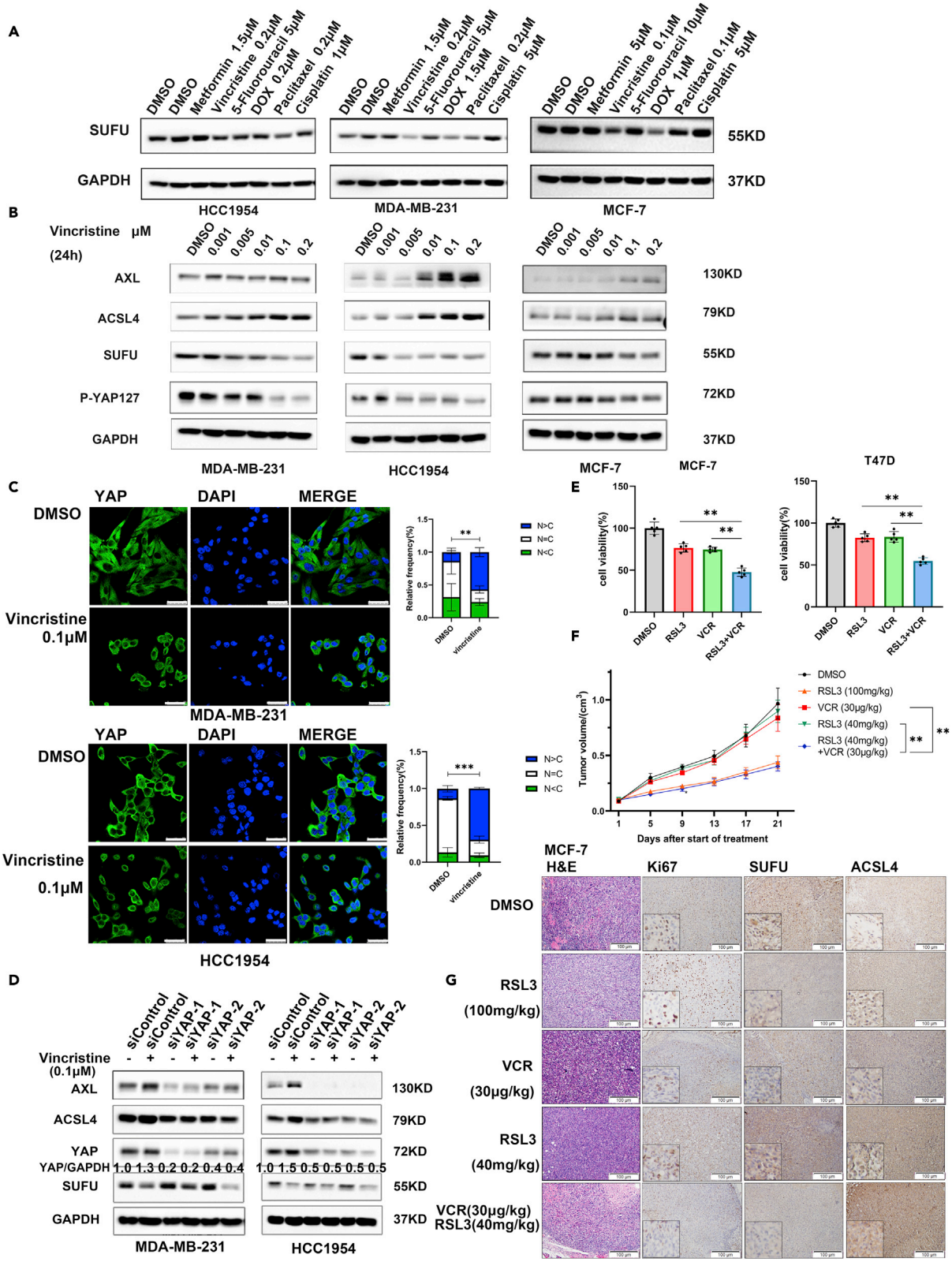
A
DMSO
DMSO
Metformin 1.5μM
Vincristine 0.2μM
5-Fluorouracil 5μM
DOX 0.2μM
Paclitaxel 0.2μM
Cisplatin 1μM
DMSO
DMSO
Metformin 1.5μM
Vincristine 0.2μM
5-Fluorouracil 5μM
DOX 1.5μM
Paclitaxel 0.2μM
Cisplatin 5μM
DMSO
DMSO
Metformin 5μM
Vincristine 0.1μM
5-Fluorouracil 10μM
DOX 1μM
Paclitaxel 0.1μM
Cisplatin 5μM
SUFU
GAPDH
55KD
37KD
HCC1954
MDA-MB-231
MCF-7
B
Vincristine μM
(24h)
DMSO 0.001 0.005 0.01 0.1 0.2
AXL
ACSL4
SUFU
P-YAP127
GAPDH
130KD
79KD
55KD
72KD
37KD
MDA-MB-231
HCC1954
MCF-7
C
YAP
DAPI
MERGE
DMSO
Vincristine 0.1μM
MDA-MB-231
HCC1954
Relative frequency(%)
N>C
N=C
N<C
DMSO
Vincristine
D
siControl
siYAP-1
siYAP-2
Vincristine (0.1μM)
AXL
ACSL4
YAP
YAP/GAPDH
SUFU
GAPDH
130KD
79KD
72KD
55KD
37KD
1.0 1.3 0.2 0.2 0.4 0.4
1.0 1.5 0.5 0.5 0.5 0.5
MDA-MB-231
HCC1954
E
MCF-7
T47D
cell viability(%)
DMSO
RSL3
VCR
RSL3+VCR
F
Tumor volume(cm3)
Days after start of treatment
DMSO
RSL3 (100mg/kg)
VCR (30μg/kg)
RSL3 (40mg/kg)
RSL3 (40mg/kg) +VCR (30μg/kg)
G
MCF-7
H&E
Ki67
SUFU
ACSL4
DMSO
RSL3 (100mg/kg)
VCR (30μg/kg)
RSL3 (40mg/kg)
VCR(30μg/kg) RSL3(40mg/kg)

Figure 6. Vincristine increases sensitivity to RSL3 via targeting SUFU-YAP-ACSL4 axis

(A) Immunoblot (IB) analysis of SUFU abundance in HCC1954, MCF-7, and MDA-MB-231 cells upon treatment with indicated compounds for 24 h. GAPDH was used as a loading control.

(B) IB analysis of SUFU, AXL, ACSL4, and P-YAP127 levels in HCC1954, MCF-7, and MDA-MB-231 cells upon treatment with increasing doses of vincristine for 24h.

(C) Confocal analysis of YAP nuclear localization in HCC1954 (lower panels) and MDA-MB-231 (upper panels) cells following the vincristine treatment for 24h; scale bar, 50μm.

(D) IB analysis showing the increase in the levels of AXL and ACSL4 in HCC1954 and MDA-MB-231 cells upon a 24 h exposure to vincristine was mitigated by siRNA-mediated knockdown of YAP.

(E) Viability (%) of MCF-7 and T47D cells treated with vehicle, vincristine, RSL3, or the combination of vincristine and RSL3.

(F) Tumor growth measurement in mouse xenograft derived from MCF-7. An intra-tumor injection was performed with vehicle, RSL3 (40 mg/kg), RSL3 (100 mg/kg) vincristine (30 μg/kg), or the combination of RSL3 (40 mg/kg) and vincristine (30 μg/kg), n = 5 in each group.

(G) Hematoxylin and eosin (H&E), Ki67, SUFU, and ACSL4-stained images of tumor tissues from tumors treated as in f; scale bar, 100μm. Data are presented as mean ± SD (*p < 0.05, **p < 0.01, ***p < 0.001, one-way ANOVA with Tukey's multiple comparisons test or Unpaired t test).

Limitations of the study

Although our study suggests that SUFU regulates the Hippo pathway in breast cancer cells via interacting with LATS1, how the interaction between SUFU and LATS1 is regulated in breast cancers remains unknown. In addition, more work is needed to dissect how this regulation impacts on SUFU-mediated ferroptosis sensitivity in breast cancers.

STAR★METHODS

Detailed methods are provided in the online version of this paper and include the following:

- KEY RESOURCES TABLE
- RESOURCE AVAILABILITY
  - Lead contact
  - Materials availability
  - Data and code availability
- EXPERIMENTAL MODEL AND SUBJECT DETAILS
  - Cell lines and plasmids
  - *In vivo* xenograft model
- METHOD DETAILS
  - Antibodies and reagents
  - Bioinformatics analysis
  - RNA interference
  - Lentiviral constructs and stable cell lines
  - Cell viability assay, crystal violet staining and SYTOX green cell death assay
  - Luciferase reporter assay
  - Lipid ROS and GSH/GSSG-Glo™ assays
  - Immunohistochemistry
  - Immunofluorescence
  - Immunoprecipitation and immunoblotting
- QUANTIFICATION AND STATISTICAL ANALYSIS

SUPPLEMENTAL INFORMATION

Supplemental information can be found online at https://doi.org/10.1016/j.isci.2022.104618.

ACKNOWLEDGMENTS

We thank Prof. D'Angiolella for kindly providing the SUFU expression constructs. professors Zengqiang Yuan, Bin Zhao, Ceshi Chen, Shian Wu, and Huadong Pei for providing expression plasmids encoding components of the Hippo pathway. This work was supported by grants from the National Natural Science Foundation of China (No. 81772973 to SM).

AUTHOR CONTRIBUTIONS

D.J., W.C., Y.W., and S.M. participated in the design of the study. K.F., S.D., D.S., Z.X., K.J., H.X., L.H., X.Z., J.W., Y.J., C.X., and Z.X. collected the data. D.L. performed bioinformatics analysis. K.F., D.S., and K.J. built

the animal model. D.L., K.F., D.J., W.C., and S.M. participated in the data analysis. Y.W. and S.M. helped to draft the manuscript. All authors read and approved the final manuscript.

DECLARATION OF INTERESTS

The authors declare no competing financial interests.

Received: January 15, 2022
Revised: May 18, 2022
Accepted: June 10, 2022
Published: July 15, 2022

REFERENCES

Alimirah, F., Peng, X., Gupta, A., Yuan, L., Welsh, J., Cleary, M., and Mehta, R.G. (2016). Crosstalk between the vitamin D receptor (VDR) and miR-214 in regulating SuFu, a hedgehog pathway inhibitor in breast cancer cells. Exp. Cell Res. *349*, 15–22. https://doi.org/10.1016/j.yexcr.2016.08.012.

Dixon, S.J., Lemberg, K.M., Lamprecht, M.R., Skouta, R., Zaitsev, E.M., Gleason, C.E., Patel, D.N., Bauer, A.J., Cantley, A.M., Yang, W.S., et al. (2012). Ferroptosis: an iron-dependent form of nonapoptotic cell death. Cell *149*, 1060–1072. https://doi.org/10.1016/j.cell.2012.03.042.

Doll, S., Proneth, B., Tyurina, Y.Y., Panzilius, E., Kobayashi, S., Ingold, I., Irmler, M., Beckers, J., Aichler, M., Walch, A., et al. (2017). ACSL4 dictates ferroptosis sensitivity by shaping cellular lipid composition. Nat. Chem. Biol. *13*, 91–98. https://doi.org/10.1038/nchembio.2239.

Dupont, S., Morsut, L., Aragona, M., Enzo, E., Giulitti, S., Cordenonsi, M., Zanconato, F., Le Digabel, J., Forcato, M., Bicciato, S., et al. (2011). Role of YAP/TAZ in mechanotransduction. Nature *474*, 179–183. https://doi.org/10.1038/nature10137.

Friedmann Angeli, J.P., Schneider, M., Proneth, B., Tyurina, Y.Y., Tyurin, V.A., Hammond, V.J., Herbach, N., Aichler, M., Walch, A., Eggenhofer, E., et al. (2014). Inactivation of the ferroptosis regulator Gpx4 triggers acute renal failure in mice. Nat. Cell Biol. *16*, 1180–1191. https://doi.org/10.1038/ncb3064.

Gao, R., Kalathur, R.K.R., Coto-Llerena, M., Ercan, C., Buechel, D., Shuang, S., Piscuoglio, S., Dill, M.T., Camargo, F.D., Christofori, G., et al. (2021). YAP/TAZ and ATF4 drive resistance to Sorafenib in hepatocellular carcinoma by preventing ferroptosis. EMBO Mol. Med. e14351. https://doi.org/10.15252/emmm.202114351.

Hangauer, M.J., Viswanathan, V.S., Ryan, M.J., Bole, D., Eaton, J.K., Matov, A., Galeas, J., Dhruv, H.D., Berens, M.E., Schreiber, S.L., et al. (2017). Drug-tolerant persister cancer cells are vulnerable to GPX4 inhibition. Nature *551*, 247–250. https://doi.org/10.1038/nature24297.

Hasegawa, M., Takahashi, H., Rajabi, H., Alam, M., Suzuki, Y., Yin, L., Tagde, A., Maeda, T., Hiraki, M., Sukhatme, V.P., et al. (2016). Functional interactions of the cystine/glutamate antiporter, CD44v and MUC1-C oncoprotein in triple-negative breast cancer cells. Oncotarget *7*, 11756–11769. https://doi.org/10.18632/oncotarget.7598.

Jiang, K., Liu, M., Lin, G., Mao, B., Cheng, W., Liu, H., Gal, J., Zhu, H., Yuan, Z., Deng, W., et al. (2016). Tumor suppressor Spred2 interaction with LC3 promotes autophagosome maturation and induces autophagy-dependent cell death. Oncotarget *7*, 25652–25667. https://doi.org/10.18632/oncotarget.8357.

Jiang, K., Liu, P., Xu, H., Liang, D., Fang, K., Du, S., Cheng, W., Ye, L., Liu, T., Zhang, X., et al. (2020). SASH1 suppresses triple-negative breast cancer cell invasion through YAP-ARHGAP42-actin axis. Oncogene *39*, 5015–5030. https://doi.org/10.1038/s41388-020-1356-7.

Kasai, K., Inaguma, S., Yoneyama, A., Yoshikawa, K., and Ikeda, H. (2008). SCL/TAL1 interrupting locus derepresses GLI1 from the negative control of suppressor-of-fused in pancreatic cancer cell. Cancer Res. *68*, 7723–7729. https://doi.org/10.1158/0008-5472.CAN-07-6661.

Kim, L.J.Y., Bhargava, S., Gimple, R.C., and Rich, J.N. (2019). SUFU: the Jekyll and Hyde of the cerebellum. Dev. Cell *48*, 131–132. https://doi.org/10.1016/j.devcel.2019.01.013.

Kraft, V.A.N., Bezjian, C.T., Pfeiffer, S., Ringelstetter, L., Müller, C., Zandkarimi, F., Merl-Pham, J., Bao, X., Anastasov, N., Kössl, J., et al. (2020). GTP cyclohydrolase 1/tetrahydrobiopterin counteract ferroptosis through lipid remodeling. ACS Cent. Sci. *6*, 41–53. https://doi.org/10.1021/acscentsci.9b01063.

Lee, Y., Kawagoe, R., Sasai, K., Li, Y., Russell, H.R., Curran, T., and McKinnon, P.J. (2007). Loss of suppressor-of-fused function promotes tumorigenesis. Oncogene *26*, 6442–6447. https://doi.org/10.1038/sj.onc.1210467.

Lin, C.C., Yang, W.H., Lin, Y.T., Tang, X., Chen, P.H., Ding, C.K.C., Qu, D.C., Alvarez, J.V., and Chi, J.T. (2021). DDR2 upregulation confers ferroptosis susceptibility of recurrent breast tumors through the Hippo pathway. Oncogene *40*, 2018–2034. https://doi.org/10.1038/s41388-021-01676-x.

Liu-Chittenden, Y., Huang, B., Shim, J.S., Chen, Q., Lee, S.J., Anders, R.A., Liu, J.O., and Pan, D. (2012). Genetic and pharmacological disruption of the TEAD-YAP complex suppresses the oncogenic activity of YAP. Genes Dev. *26*, 1300–1305. https://doi.org/10.1101/gad.192856.112.

Liu, M., Jiang, K., Lin, G., Liu, P., Yan, Y., Ye, T., Yao, G., Barr, M.P., Liang, D., Wang, Y., et al. (2018). Ajuba inhibits hepatocellular carcinoma cell growth via targeting of beta-catenin and YAP signaling and is regulated by E3 ligase Hakai through neddylation. J. Exp. Clin. Cancer Res. *37*, 165. https://doi.org/10.1186/s13046-018-0806-3.

Poursaitidis, I., Wang, X., Crighton, T., Labuschagne, C., Mason, D., Cramer, S.L., Triplett, K., Roy, R., Pardo, O.E., Seckl, M.J., et al. (2017). Oncogene-selective sensitivity to synchronous cell death following modulation of the amino acid nutrient cystine. Cell Rep. *18*, 2547–2556. https://doi.org/10.1016/j.celrep.2017.02.054.

Raducu, M., Fung, E., Serres, S., Infante, P., Barberis, A., Fischer, R., Bristow, C., Thézénas, M., Finta, C., Christianson, J.C., et al. (2016). SCF (Fbxl17) ubiquitylation of Sufu regulates Hedgehog signaling and medulloblastoma development. EMBO J. *35*, 1400–1416. https://doi.org/10.15252/embj.201593374.

Skubnik, J., Pavlíčková, V.S., Ruml, T., and Rimpelová, S. (2021). Vincristine in combination therapy of cancer: emerging trends in clinics. Biology *10*, 849. https://doi.org/10.3390/biology10090849.

Stockwell, B.R., Jiang, X., and Gu, W. (2020). Emerging mechanisms and disease relevance of ferroptosis. Trends Cell Biol. *30*, 478–490. https://doi.org/10.1016/j.tcb.2020.02.009.

Wu, J., Minikes, A.M., Gao, M., Bian, H., Li, Y., Stockwell, B.R., Chen, Z.N., and Jiang, X. (2019). Publisher Correction: intercellular interaction dictates cancer cell ferroptosis via NF2-YAP signalling. Nature *572*, E20. https://doi.org/10.1038/s41586-019-1480-0.

Yang, W.H., and Chi, J.T. (2020). Hippo pathway effectors YAP/TAZ as novel determinants of ferroptosis. Mol. Cell Oncol. *7*, 1699375. https://doi.org/10.1080/23723556.2019.1699375.

Yang, W.H., Ding, C.K.C., Sun, T., Rupprecht, G., Lin, C.C., Hsu, D., and Chi, J.T. (2019). The Hippo pathway effector TAZ regulates ferroptosis in renal cell carcinoma. Cell Rep. *28*, 2501–2508.e4. https://doi.org/10.1016/j.celrep.2019.07.107.

Yang, W.H., Huang, Z., Wu, J., Ding, C.K.C., Murphy, S.K., and Chi, J.T. (2020). A TAZ-ANGPTL4-NOX2 Axis regulates ferroptotic cell death and chemoresistance in epithelial ovarian cancer. Mol. Cancer Res. *18*, 79–90. https://doi.org/10.1158/1541-7786.MCR-19-0691.

Yang, W.H., Lin, C.C., Wu, J., Chao, P.Y., Chen, K., Chen, P.H., and Chi, J.T. (2021). The Hippo pathway effector YAP promotes ferroptosis via

the E3 ligase SKP2. Mol. Cancer Res. *19*, 1005–1014. https://doi.org/10.1158/1541-7786.MCR-20-0534.

Yang, W.S., SriRamaratnam, R., Welsch, M.E., Shimada, K., Skouta, R., Viswanathan, V.S., Cheah, J.H., Clemons, P.A., Shamji, A.F., Clish, C.B., et al. (2014). Regulation of ferroptotic cancer cell death by GPX4. Cell *156*, 317–331. https://doi.org/10.1016/j.cell.2013.12.010.

Yang, W.S., and Stockwell, B.R. (2008). Synthetic lethal screening identifies compounds activating iron-dependent, nonapoptotic cell death in oncogenic-RAS-harboring cancer cells. Chem. Biol. *15*, 234–245. https://doi.org/10.1016/j.chembiol.2008.02.010.

Yi, J., Zhu, J., Wu, J., Thompson, C.B., and Jiang, X. (2020). Oncogenic activation of PI3K-AKT-mTOR signaling suppresses ferroptosis via SREBP-mediated lipogenesis. Proc. Natl. Acad. Sci. U S A *117*, 31189–31197. https://doi.org/10.1073/pnas.2017152117.

Zhang, X., Yu, K., Ma, L., Qian, Z., Tian, X., Miao, Y., Niu, Y., Xu, X., Guo, S., Yang, Y., et al. (2021). Endogenous glutamate determines ferroptosis sensitivity via ADCY10-dependent YAP suppression in lung adenocarcinoma. Theranostics *11*, 5650–5674. https://doi.org/10.7150/thno.55482.

Zhang, Y., Tan, H., Daniels, J.D., Zandkarimi, F., Liu, H., Brown, L.M., Uchida, K., O'Connor, O.A., and Stockwell, B.R. (2019). Imidazole ketone erastin induces ferroptosis and slows tumor growth in a mouse lymphoma model. Cell Chem. Biol. *26*, 623–633.e9. https://doi.org/10.1016/j.chembiol.2019.01.008.

Zhao, B., Li, L., Tumaneng, K., Wang, C.Y., and Guan, K.L. (2010). A coordinated phosphorylation by Lats and CK1 regulates YAP stability through SCF(beta-TRCP). Genes Dev. *24*, 72–85. https://doi.org/10.1101/gad.1843810.

Zhao, B., Wei, X., Li, W., Udan, R.S., Yang, Q., Kim, J., Xie, J., Ikenoue, T., Yu, J., Li, L., et al. (2007). Inactivation of YAP oncoprotein by the Hippo pathway is involved in cell contact inhibition and tissue growth control. Genes Dev. *21*, 2747–2761. https://doi.org/10.1101/gad.1602907.

Zhao, B., Ye, X., Yu, J., Li, L., Li, W., Li, S., Yu, J., Lin, J.D., Wang, C.Y., Chinnaiyan, A.M., et al. (2008). TEAD mediates YAP-dependent gene induction and growth control. Genes Dev. *22*, 1962–1971. https://doi.org/10.1101/gad.1664408.

STAR★METHODS

KEY RESOURCES TABLE

REAGENT or RESOURCE	SOURCE	IDENTIFIER
Antibodies		
SUFU	Cell Signaling Technology	C81H7; AB_2302728
LATS1	Cell Signaling Technology	3477S; AB_2133513
P-LATS1	Cell Signaling Technology	9157S; AB_2133515
P-YAP127	Cell Signaling Technology	4911S; AB_2218913
V5-tag	Cell Signaling Technology	13202S; AB_2687461
Myc-tag	Cell Signaling Technology	2278S; AB_490778
xCT/SLC7A11	Cell Signaling Technology	12691; AB_2687474
Anti-V5	Invitrogen Thermo Fisher Scientific	46-0705; AB_10804584
YAP1	NOVUS	NB110-58358; AB_922796
GAPDH	Proteintech	10494-1-AP; AB_2263076
AXL	Proteintech	13196-1-AP; AB_10642006
Flag-tag	Proteintech	20543-1-AP; AB_11232216
HA-tag	Sigma	H6908; AB_260070
LAMIN A+C	Abcam	ab133256; AB_2813767
ACSL4	Abcam	ab155282; AB_2714020
GPX4	Abcam	ab125066; AB_10973901
Ki67	Abcam	ab16667; AB_302459
SUFU	Santa Cruz Biotechnology	sc-137014; AB_2197315
IgG	Santa Cruz Biotechnology	sc-69786; AB_1124809
Chemicals, peptides, and recombinant proteins		
Verteporfin	Selleck	S1786; CAS: 129497-78-5
Z-VAD-FMK	Selleck	S7023; CAS: 187389-52-2
Necrostatin-1	Selleck	S8037; CAS: 4311-88-0
Ferrostatin-1	Sigma	SML0583; CAS: 347174-05-4
liproxstatin-1	Sigma	SML1414; CAS: 950455-15-9
1S,3R-RSL3	Sigma	SML2234; CAS: 1219810-16-8
Doxorubicin Hydrochloride	Sigma	D1515; CAS: 25316-40-9
3-Methyladenine	CALBIOCHEM	189490; CAS: 5142-23-4
Metformin	TargetMol	T0740; CAS: 1115-70-4
Vincristine	J&K Scientific	594515; CAS: 2068-78-2
5-Fluorouracil	Aladdin	51-21-8; CAS: 51-21-8
Paclitaxel	Solarbio	SP8020; CAS: 33069-62-4
Cisplatin	Solarbio	SC5170; CAS: 15663-27-1
Critical commercial assays		
CCK8	MedChemExpress	Cat#HY-K0301
Sytox Green staining	Thermo	Cat#S34860
Dual-Luciferase Reporter Assay System	Promega	Cat# E1910
BODIPY 581/591 C11 (Lipid Peroxidation Sensor)	Thermo	Cat# D3861
GSH/GSSG-Glo™ assay	Promega	Cat# V6911
Deposited data		

(*Continued on next page*)

Continued

REAGENT or RESOURCE	SOURCE	IDENTIFIER
Raw and analyzed data (mRNA-seq)	This paper	GEO:GSE188806
Experimental models: Cell lines		
HCC1954	ATCC	CRL-2338
MDA-MB-231	ATCC	HTB-26
MCF-7	ATCC	HTB-22
SK-BR-3	ATCC	HTB-30
T47D	ATCC	HTB-133
293T	ATCC	CRL-11268
MCF-10A	ATCC	CRL-10317
MDA-MB-468	ATCC	HTB-132
HCC1806	ATCC	CRL-2335
HCC1937	ATCC	CRL-2336
Experimental models: Organisms/strains		
BALB/c Nude mice	Beijing Vital River Laboratory Animal Technology Co., Ltd	N/A
Oligonucleotides		
V5-SUFU-WT Forward: 5′-AGAA GCTTATGGCGGAGCTGCGGC-3′	This paper	N/A
V5-SUFU-WT Reverse: 5′-CGGGAT CCGTGTAGCGGACTGTCGAACAC-3′	This paper	N/A
V5-SUFU-d(1–173) Forward: 5′-AGAAGC TTATGATTCAGCACATGCTGCTGACA-3′	This paper	N/A
V5-SUFU-d(1–173) Reverse: 5′-CGGGATCC GTGTAGCGGACTGTCGAACAC-3′	This paper	N/A
V5-SUFU-d (174–385) Forward: 5′-CAGGA GCCTGCCCCTTCTTGACTCACTGTT-3′	This paper	N/A
V5-SUFU-d (174–385) Reverse: 5′-AACAGTG AGTCAAGAAGGGGCAGGCTCCTG-3′	This paper	N/A
V5-SUFU-d(386–484) Forward: 5′-AGAAG CTTATGGCGGAGCTGCGGC-3′	This paper	N/A
V5-SUFU-d(386–484) Reverse: 5′-CGGGAT CCTAGGCAGAGAGGAATGAGGGC-3′	This paper	N/A
V5-SUFU-d(1–173)+ (386–484) Forward: 5′-AG AAGCTTATGATTCAGCACATGCTGCTGACA-3′	This paper	N/A
V5-SUFU-d(1–173)+ (386–484) Reverse: 5′-CGG GATCCTAGGCAGAGAGGAATGAGGGC-3′	This paper	N/A
siRNA targeting sequence: siSUFU-1: 5′-CCU CAUUCCUCUCUGCCUATT-3′	Ribobio(Guangzhou, China)	N/A
siRNA targeting sequence: siSUFU-2:5′-GGAG AGGACUCGAGAUCAATT-3′	Ribobio(Guangzhou, China)	N/A
siRNA targeting sequence: siYAP-1:5′-GAC AUCUUCUGGUCAGAGA-3′	Ribobio(Guangzhou, China)	N/A
siRNA targeting sequence: siYAP-2:5′-GA GATGGAATGAACATAGA-3′	Ribobio(Guangzhou, China)	N/A
siRNA targeting sequence: siACSL4-1:5′-GA GCGATTTGAAATTCCAA-3′	Ribobio(Guangzhou, China)	N/A
siRNA targeting sequence: siACSL4-2:5′-ACA GCATGCAATCAGTAGA-3′	Ribobio(Guangzhou, China)	N/A

(*Continued on next page*)

Continued

REAGENT or RESOURCE	SOURCE	IDENTIFIER
Recombinant DNA		
Myc-LATS1 pcDNA3.1 plasmid	This paper	N/A
Myc-LATS2 pcDNA3.1 plasmid	This paper	N/A
Myc-YAP pcDNA3.1 plasmid	This paper	N/A
Myc-SAV1 pcDNA3.1 plasmid	This paper	N/A
Myc-MOB1 pcDNA3.1 plasmid	This paper	N/A
HA-Kibra pcDNA3.1 plasmid	This paper	N/A
HA-Merlin pcDNA3.1 plasmid	This paper	N/A
Flag-MST1 pcDNA3.1 plasmid	This paper	N/A
Flag-MST2 pcDNA3.1 plasmid	This paper	N/A
V5-SUFU-WT pcDNA3.1 plasmid	This paper	N/A
Flag-SUFU-WT pcDNA3.1 plasmid	This paper	N/A
V5-SUFU-d(1–173) pcDNA3.1 plasmid	This paper	N/A
V5-SUFU-d(386–484) pcDNA3.1 plasmid	This paper	N/A
V5-SUFU-d(174–385) pcDNA3.1 plasmid	This paper	N/A
V5-SUFU-d(1–173)+ d(386–484) pcDNA3.1 plasmid	This paper	N/A
Software and algorithms		
ImageJ	Schneider et al., 2012	https://imagej.nih.gov/ij
GraphPad Prism 9.0	GraphPad Prism Software, Inc	https://www.graphpad.com/
Adobe Photoshop CS6	Adobe	N/A
Other		
Trizol	Invitrogen	Cat#15596018

RESOURCE AVAILABILITY

Lead contact

Further information and requests for resources and reagents should be directed to and will be fulfilled by the lead contact, Songshu Meng (ssmeng@dmu.edu.cn).

Materials availability

This study did not generate new unique reagents and all materials in this study are commercially available.

Data and code availability

- Data: All data reported in this paper will be shared by the lead contact upon request.
- Code: This paper does not report original code.
- Additional information: Any additional information required to reanalyze the data reported in this paper is available from the lead contact upon reasonable request.

EXPERIMENTAL MODEL AND SUBJECT DETAILS

Cell lines and plasmids

Human breast cancer cell lines HCC1954, HCC1806, HCC1937, MCF-7, MDA-MB-231, MDA-MB-468, SK-BR-3, and T47D, human mammary epithelial cell line MCF-10A and human embryonic kidney (293T) cell line were purchased from the American Type Culture Collection. Cells were cultured at 37°C in 5% CO_2 with DMEM or RPMI-1640 (Gibco) medium supplemented with 10% fetal bovine serum, 100 unit/mL penicillin and 100 mg/mL streptomycin. MCF-10A cells were in the DMEM/F12 media (Invitrogen) supplemented with horse serum (5% final, Invitrogen) insulin (10 μg/ml, Sigma), EGF (20 ng/ml, Peprotech), hydrocortisone (0.5 μg/ml, Sigma), 1% penicillin–streptomycin (Invitrogen), and cholera toxin (100 ng/ml, Sigma).

The HA-tagged SUFU cDNA construct was kindly provided by Prof. Vincenzo D'Angiolella (Raducu et al., 2016). V5 or Flag-tagged SUFU wild type and deletion mutants were constructed by standard molecular cloning procedures.

In vivo xenograft model

All animal studies were carried out at Dalian Medical University Laboratory Animal Center, and conducted in accordance with the national guidelines for the care and use of laboratory animals with approval from the experimental animal ethics committee: Dalian Medical University.

For subcutaneous tumor formation, MDA-MB-231 cells (1 × 107) were injected subcutaneously into flanks of nude mice (female, 5–6 weeks-old, n = 5, Beijing Vital River Laboratory Animal Technology Co., Ltd). Tumor diameters were measured every three days and the tumor volume was calculated using the equation: V = 0.52×L×W2. Tumor-bearing mice were euthanized by CO2 inhalation at the tumor burden endpoint.

For RSL3 and vincristine combination experiments, MCF-7 cells (1 × 107) were implanted subcutaneously into the flank of 5-to 6-week-old nude mice. Mice with established tumors with approximately 50–80 mm3 average volumes were randomized into treatment groups (n = 5), including vehicle (DMSO), RSL3 (100 mg/kg in 20mL DMSO plus 80mL corn oil), RSL3 (40 mg/kg), vincristine (30 μg/kg), or the combination of RSL3 (40 mg/kg) with vincristine (30 μg/kg). Compounds or vehicle were administered through intra-tumor injection biweekly.

METHOD DETAILS

Antibodies and reagents

The following antibodies were purchased from Cell Signaling Technology (America): SUFU (C81H7), LATS1 (3477S), P-LATS1 (9157S), P-YAP127 (4911S), V5-tag (13202S), Myc-tag (2278S), xCT/SLC7A11 (12691). Anti-V5 (P/N46-0705) was obtained from Invitrogen Thermo Fisher Scientific (America). YAP1 (NB110-58358) was purchased from NOVUS (America). GAPDH (10494-1-AP), AXL (13196-1-AP) and Flag-tag (20543-1-AP) were bought from Proteintech (America). HA-tag (H6908) was purchased from Sigma (America). LAMIN A + C (ab133256), ACSL4 (ab155282), GPX4 (ab125066) and Ki67 (ab16667) were bought from Abcam (UK). SUFU (sc-137014) and IgG (sc-69786) were purchased from Santa Cruz Biotechnology (America). Verteporfin (S1786), Z-VAD-FMK (S7023) and Necrostatin-1 (S8037) were purchased from Selleck Chemicals (America). Ferrostatin-1 (SML0583), liproxstatin-1 (SML1414), 1S,3R-RSL3 (SML2234) and Doxorubicin Hydrochloride (D1515) were obtained from Sigma (America). 3-Methyladenine (189490) was bought from CALBIOCHEM (Germany). Metformin (T0740) was purchased from TargetMol (America). Vincristine (594515) was bought from J&K Scientific (China). 5-Fluorouracil (51-21-8) was obtained from Aladdin (China). Paclitaxel (SP8020) and Cisplatin (SC5170) were purchased from Solarbio (China). Drugs were dissolved and stored at − 20°C or −80°C according to the manufacturer's instructions.

Bioinformatics analysis

For pharmaco-transcriptomic correlation analysis, gene expression data of human solid cancer cell lines were obtained from the Cancer Cell Line Encyclopedia (CCLE) project. The CTRP2.0 contains the sensitivity data for ferroptosis inducers (erastin, sorafenib, RSL3, ML162, ML210) and provides area under the curve (AUC), determined by fitted concentration-response curves (2-fold dilution, over a 16-point concentration range), as a measure of drug sensitivity. AUC values were rescaled into a range of [0, 1] (AUC/30). Pearson correlation was calculated between SHH signaling gene expression and ferroptosis inducers AUC.

RNA-Seq was performed by the Novogene Corporation (Beijing, China). The sequencing libraries were constructed using NEBNext® UltraTM RNA Library Prep Kit for Illumina® (NEB, USA) according to the manufacturer's instructions. The heatmap of differentially expressed genes (DEGs) was generated using the R ComplexHeatmap package. The association between SUFU and YAP was analyzed with Gene Set Enrichment Analysis (GSEA) using YAP-dependent gene signatures collected from YAP common MCF10 and 3T3_Zhao (Zhao et al., 2008). Metrics for ranking the key mRNAs were calculated based on log2 fold change in SUFU knockdown vs control. YAP dependent gene signatures were significantly enriched at p-value < 0.05 and q-value < 0.25.

RNA-sequencing (RNA-seq) for transcriptional profiles of SKBR3 control and SUFU-overexpressing cells (GSE188806) and HCC1954 control and cells with SUFU silencing (GSE188806) have been deposited in the NCBI Genome Expression Omnibus under SuperSeries GSE 188806. Differentially expressed genes upon overexpression of SUFU compared to control in SK-BR-3 cells are listed in Table S1. Differentially expressed genes upon knockdown of SUFU compared to control in HCC1954 cells are listed in Table S2. Geneset enrichment analysis (GSEA) of YAP gene set upon knockdown of SUFU in HCC1954 cells is listed in Table S3.

RNA interference

siRNA oligonucleotides were purchased from Ribobio (Guangzhou, China) and sequences are as follows:

siSUFU-1: 5′-CCUCAUUCCUCUCUGCCUATT-3′

siSUFU-2: 5′-GGAGAGGACUCGAGAUCAATT-3′

siYAP-1: 5′-GACAUCUUCUGGUCAGAGA-3′

siYAP-2: 5′-GAGATGGAATGAACATAGA-3′

siACSL4-1: 5′-GAGCGATTTGAAATTCCAA-3′

siACSL4-2: 5′-ACAGCATGCAATCAGTAGA-3′

siRNAs or negative control (siControl) were transfected with Lipofectamine 3000 (Invitrogen) according to the manufacturer's instructions.

Lentiviral constructs and stable cell lines

The lentiviral vectors encoding short hairpin RNAs (GIPZ shRNAs) targeting SUFU, LATS1, and ACSL4, respectively, and scrambled shRNA were purchased from Dharmacon (America). Flag-tagged SUFU was subcloned into the pCDH-puro lentiviral vector by standard molecular cloning procedures. Stable cell lines knocking down or overexpressing SUFU were established. LATS1-depleted MDA-MB-231 cells were established in our lab (Jiang et al., 2020).

Cell viability assay, crystal violet staining and SYTOX green cell death assay

Cells were seeded (2000cells/well) in 96-well plates for the indicated time, and cell viability was measured by Cell Counting Kit-8 (CCK8, MCE/Y-K0301) or Crystal violet staining. For IC50 assays, a CCK-8 assay was used to measure drug sensitivity at 450 nm using a microplate reader (Thermo Fisher Scientific).

Cytotoxicity was determined by Sytox Green staining (Thermo) according to the manufacturer's protocol. To analyse cell death, breast cancer cells were seeded at 2×10^5 cells/well into 12-well plates. After 24h contact, cells were divided into control group and model group. In the control group, cells were incubated for 24h in complete medium; In the RSL3 group, cells were incubated in the same medium with the presence of RSL3. Following incubation, cells were rinsed twice with PBS. Then adhered cells were incubated with SYTOX Green staining solution (40 nM) in PBS in the dark for 30 minutes at 37°C. Cells were rinsed twice with PBS and imaged by inverted fluorescence microscope.

Luciferase reporter assay

For the luciferase assays, cells at 50% confluency were transfected in 24-well plates with 0.1μg of a YAP/TAZ-responsive luciferase gene (8xGTIIC-luciferase reporter) or empty vector control (pGL3), with 0.1μg of pcDNA3.1 empty vector or pcDNA3.1-V5-SUFU and 0.02μg pRL-TKRenilla (Promega) as a transfection control. The cells were lysed in 50μL passive lysis buffer for 3 days after transfection. The soluble fraction was subsequently assayed for luciferase activity with a Dual-Luciferase Reporter Assay System (Promega, USA).

Lipid ROS and GSH/GSSG-Glo™ assays

Lipid ROS levels in breast cancer cells were assessed by BODIPY 581/591 C11 (lipid peroxidation sensor, Thermo scientific, USA) according to the manufacturer's instructions. To analyse lipid peroxidation, breast cancer cells were seeded at 5×10^5 cells/well into 6-well plates. After 24h contact, cells were divided into

two groups, the control group and the model group. In the control group, cells were incubated for 24h in complete medium; In the RSL3 group, cells were incubated in the same medium with the presence of RSL3. Following incubation, the cells were rinsed twice with PBS. Adhered cells were incubated with C11-BODIPY (5 μM) staining solution in PBS in the dark for 30 minutes at 37°C. Cells were then harvested with 0.05% trypsin solution, suspended in fresh medium, and immediately analyzed with flow cytometer. Each sample test was repeated in three independent wells.

Detection and quantification of the GSH/GSSG ratios were carried out with GSH/GSSG-Glo™ assay (Promega, Southampton, UK) according to the manufacturer's guidelines.

Immunohistochemistry

Paraffin-embedded tissue sections were dewaxed using a decreasing xylene/alcohol series. Briefly, the processed sections were blocked with 3% BSA and incubated with anti-SUFU antibody (1:50) and anti-ACSL4 antibody (1:100). The DAB Detection Kit was used to develop the staining signals according to the protocols provided for the streptavidin-peroxidase system (Sangon Biotech, China). Haematoxylin was used for counterstaining.

Immunofluorescence

Seed and allow cells to adhere to glass slides in the cell culture medium for 24 h and fixed with 4% paraformaldehyde (PFA) for 20 minutes. To visualize cytoplasmic and nuclear components, 4% PFA fixed cells were permeabilized with 0.5% Triton X-100 for 20 minutes. Then the cells were blocked with 5% BSA for 60 minutes. Primary antibodies were diluted in blocking buffer and cells were incubated overnight at 4°C. Cells were washed with PBS and fluorescently labeled secondary antibodies were diluted in blocking buffer followed by incubation for 30 minutes at room temperature. Finally, the cells were sealed with anti-fluorescence quenching sealing tablets.

Immunoprecipitation and immunoblotting

For immunoprecipitation studies, cells were harvested 24 hours after being transfected with plasmids in 1% Triton X-100 lysis buffer, which was supplemented with a mixture of protease and phosphatase inhibitors. Lysates were centrifuged and supernatants collected. Supernatants were precipitated by 30μL of protein G dynabeads (Roche, 11243233001) for one hour followed by 4°C incubation with rotation for 2.5 hours in the presence of 5 μg/ml antibodies or control IgG. Immunoprecipitated complexes were washed five times with cold lysis buffer before boiling in 1X Loading Buffer. Immunoprecipitates and 2% lysate loading controls were then run on an SDS-PAGE gel and subsequent immunoblotting was conducted.

For immunoblotting (IB), *in vitro* cultured human brest cancer cells were harvested using RIPA lysis buffer (10mM Tris-HCl, pH 8.0, 140mM NaCl, 1mM EDTA, 1% Triton X-100, 0.1% sodium deoxycholate, 0.1% SDS, pH 7.4) supplemented with a cocktail of protease and phosphatase inhibitors. The protein concentrations were assessed using a BCA Protein Assay reagent kit, and after boiling, protein samples were separated via sodium dodecyl sulfate–polyacrylamide gel electrophoresis. Then, proteins were transferred onto a nitrocellulose membrane using electrophoresis (Bio-Rad Laboratories). All membranes were blocked with 5% nonfat dry milk in 1× Tris-buffered saline with Tween 20 for 1 hour and then incubated at 4°C overnight with the primary antibodies: After washing with 1×Tris-buffered saline with Tween 20, membranes were then incubated with horseradish peroxidase–conjugated anti-mouse or anti-rabbit immunoglobulin G for 1 hour at room temperature and exposed using an enhanced ECL Western Blotting Substrate. GAPDH was used as loading control (Jiang et al., 2016, 2020; Liu et al., 2018), and the detailed information about antibodies were provided in key resources table.

QUANTIFICATION AND STATISTICAL ANALYSIS

All data analyses in this experiment were performed by GraphPad Prism 7 software. Differences between variables of two groups were examined by Student's *t* test, and one-way ANOVA was used to evaluate the differences among variables of multiple groups. The results were shown as mean ± standard error. Significant difference: $*p < 0.05$, $**p < 0.01$, $***p < 0.001$.